

LOCAL PHOTODYNAMIC THERAPY FOR EQUINE  
SQUAMOUS CELL CARCINOMA IN A MURINE MODEL

---

A Thesis presented to the Faculty of the Graduate School  
University of Missouri-Columbia

---

In Partial Fulfillment  
Of the Requirements for the Degree  
Master of Biomedical Sciences

---

By  
Juri Ota  
Dr. Elizabeth A. Giuliano, Thesis Supervisor  
May 2007

The undersigned, appointed by the dean of the Graduate School, have examined the thesis entitled

**LOCAL PHOTODYNAMIC THERAPY FOR SQUAMOUS CELL CARCINOMA  
IN A MURINE MODEL**

Presented by Juri Ota

A candidate for the degree of Master of Biomedical Sciences

And hereby certify that, in their opinion, it is worthy of acceptance.

---

Dr. Elizabeth A. Giuliano

---

Dr. Leah A. Cohn

---

Dr. Michael R. Lewis

---

Dr. Cecil P. Moore

## **ACKNOWLEDGEMENTS**

The author wishes to thank the following individuals:

Dr. Elizabeth Giuliano, for her unwavering support and mentorship in this research and clinical ophthalmology residency program.

Drs. Leah A. Cohn and Michael R. Lewis, for their mentorship and guidance in basic science research training.

Dr. Cecil P. Moore, for his mentorship and generous support during my clinical ophthalmology residency program.

Dr. Richard D. Madsen, for statistical assistance.

Ms. Marilyn Beissenherz, for her technical assistance in immunohistochemistry.

Mr. Don Connor and Mr. Howard Wilson, for technical support.

Supported by grants from the American College of Veterinary Ophthalmologists - Vision for Animals, University of Missouri, Phi Zeta Society and the University of Missouri, College of Veterinary Medicine, Committee on Research.

## TABLE OF CONTENTS

ACKNOWLEDGEMENTS .....	ii
LIST OF TABLES .....	v
LIST OF FIGURES .....	vi
CHAPTER 1 INTRODUCTION	
1. Equine Ocular Squamous Cell Carcinoma .....	1
2. Murine Tumor Model .....	2
3. Tissue Cryopreservation .....	3
4. Photodynamic Therapy .....	4
a. Overview .....	4
b. Photochemistry of photodynamic therapy .....	4
c. Biologic mechanisms of action .....	5
d. Photosensitizer localization .....	8
e. Photosensitizers .....	8
f. Light source and delivery .....	10
CHAPTER 2 EXPERIMENTAL PURPOSE AND HYPOTHESIS .....	11
CHAPTER 3 DEVELOPMENT OF MURINE MODEL FOR EQUINE OCULAR SQUAMOUS CELL CARCINOMA	
1. Material and Methods	
a. Animals .....	13
b. Tumor collection and cyropreservation .....	14
c. Cell viability test .....	14
d. Transplantation of equine tumor .....	15
e. Histopathological examination .....	16

2. Results	
a. Cell viability.....	17
b. Tumor implantation efficiency and growth rate .....	18
c. Histopathologic evaluation.....	18
3. Discussion.....	19
CHAPTER 4 LOCAL PHOTODYNAMIC THERAPY FOR SQUAMOUS CELL CARCINOMA IN A MURINE MODEL	
1. Materials and Methods	
a. Animals .....	26
b. Tumor model.....	26
c. Photosensitizer .....	27
d. Light delivery system.....	27
e. Experimental protocol.....	28
i. Experimental A: The effect of drug dose.....	28
ii. Experimental B: The effect of drug solvent .....	29
2. Results.....	30
3. Discussion.....	33
APPENDIX	
TABLES .....	40
FIGURES .....	41
BIBLIOGRAPHY.....	51

## LIST OF TABLES

### Tables

1. Origin of equine SCC tumor .....	40
2. Experiment A – effect of photoactive drug dose .....	40
3. Experiment B – effect of solvent .....	40

## LIST OF FIGURES

Figures	Page
1. Jablonski diagram.....	41
2. (A) Confocal microscopy image of cryopreserved equine ocular SCC from of the original equine patients, x 4. ....	42
(B) Confocal microscopy image of cryopreserved equine ocular SCC from one of the original equine patients x 20. ....	42
3. The SCID mouse bearing equine SCC 138 days following implantation .....	42
4. Growth curve of xenotransplanted equine SCC .....	42
5. (A) Histopathology of SCC from an original equine patient, hematoxylin eosin stain, x 400. ....	43
(B) Immunohistochemical staining for cytokeratin 5/6 on SCC from an original equine patient, x 400.....	43
(C) Histopathology of cryopreserved equine SCC, hematoxylin-eosin stain, x 400.....	43
(D) Immunohistochemical staining for cytokeratin 5/6 on a cryopreserved equine SCC, x 400 .....	43
(E) Histopathology of an equine SCC xenograft harvested on day 150 from a SCID mouse, hematoxylin-eosin stain, x 400. The tumor was well circumscribed, restricted to the subcutaneous space with central necrosis. Histologic pattern was identical to the original equine tumor .....	43
(F) Immunohistochemical staining for cytokeratin 5/6 on a SCC xenograft, x 400. Diffuse and strong positive immunohistochemical stain for cytokeratin 5/6 remained the same in its intensity and location as the original equine SCC.....	43
6. Immunoreactivity for p53 on original (Figure A) cryopreserved (Figure B), and transplanted (Figure C) ocular SCC. Nonimmune control (Figure D).....	44
7. A photograph of a xenografted nude mouse under general anesthesia being illuminated with LED light after local injection with verteporfin .....	45

8.	A photograph of an ulcer formed in the treatment site following PDT with local injection of verteporfin at a dose of 0.1 mg/cm <sup>3</sup> .....	45
9.	Comparison of tumor growth in Experiment A .....	46
10.	Comparison of tumor growth in Experiment B .....	47
11.	Mean relative change in tumor volume at day 13 of mice in experiment A.....	48
12.	Mean relative change in tumor volume at day 30 of mice in experiment B.....	48
13.	Mean relative change in tumor volume at day 13 of mice in experiment B.....	49
14.	Mean relative change in tumor volume at day 30 of mice in experiment B.....	49
15.	Photographs of mouse in treatment group B2 demonstrating complete regression of SCC.....	50



# CHAPTER 1

## INTRODUCTION

### 1. EQUINE OCULAR SQUAMOUS CELL CARCINOMA

Squamous cell carcinoma (SCC) is the most common neoplasm of the equine eye and ocular adnexa and the second most common tumor of the horse overall.<sup>1, 2</sup> Ocular SCC may involve the corneconjunctiva, bulbar conjunctiva, third eyelid and eyelids.<sup>3</sup> Biological behavior of SCC is reported to differ depending on location, but it is typically locally invasive with a potential to metastasize. Poorer prognosis was associated with tumor located at the eyelid, compared to the third eyelid, nasal canthus or limbus in one study.<sup>4</sup> Metastasis of ocular SCC to local lymph nodes, salivary glands, and lungs can occur. Reported rates of metastasis for equine ocular SCC range from 6 to 15.4 %.<sup>5, 6</sup> Local invasion of the tumor often accompanies ulcerative necrosis and inflammation resulting in significant ocular discomfort.

A variety of treatment modalities for equine SCC has been reported in case reports or case series with variable success. Reported therapies include surgical excision<sup>7</sup>, cryotherapy<sup>8</sup>, beta-irradiation<sup>9, 10</sup>, radiofrequency hyperthermia<sup>11</sup>, intratumoral chemotherapy<sup>12</sup>, and interstitial radiotherapy.<sup>13</sup> Recurrence rates within a year of treatment have been reported between 50-66.7% with surgery alone, and range from 15-67% with surgery and ancillary irradiation or cryotherapy.<sup>3, 14</sup> A 42.4 % recurrence rate for ocular SCC with surgical excision, radiofrequency hyperthermia or both has also been reported.<sup>6</sup> In another study, treatments included surgical excision, surgical excision with <sup>90</sup>Sr beta irradiation, surgical excision with cryotherapy, surgical excision with

radiofrequency, surgical excision with  $^{137}\text{Cs}$  interstitial radiotherapy, and/or immunotherapy, and the overall recurrence rate was 30.4%.<sup>4</sup> No single treatment modality has proven to be effective, and treatment complications commonly threaten both visual outcome and long term survival. In an effort to preserve vision and comfort, much effort has been directed toward improving adjuvant therapy following surgical excision. However, ocular SCC in horses is a spontaneously occurring disease, and the use of horses to prospectively evaluate treatment response rates to new therapeutic modalities is both cost prohibitive and limited by animal numbers. To date, a clinically relevant *in vivo* model for equine SCC does not exist.

## **2. MURINE TUMOR MODEL**

Murine tumor models which accurately reproduce spontaneous neoplasia play important roles in investigating tumor behavior, histological characteristics, and in evaluating efficacy of novel cancer treatments. Studies using these models provide advantages of reproducibility of the neoplasia, low cost, ease of manipulation and time effectiveness. Xenografts of animal tumors may represent metabolic characteristics of animal malignant disease and often have value in selecting tumor-specific agents when used as screening tools.<sup>15</sup> Studies have shown that tumor xenografts in murine models demonstrate a significant correlation with clinically relevant response rates to various treatments.<sup>16</sup>

In veterinary oncology research, subcutaneous induction of tumor growth in mice has been described following xenotransplantation from dogs (mammary carcinoma<sup>17</sup>, non-small cell lung cancers<sup>18</sup>, mast cell tumor<sup>19</sup>, lymphomas<sup>20,21</sup>, transmissible venereal

tumor<sup>22,23</sup>, glioma<sup>23</sup>), cats (mammary carcinoma<sup>24</sup>, melanoma<sup>25</sup>), cows (lymphosarcoma<sup>26</sup>), and sheep (squamous cell carcinoma<sup>27</sup>). Such transplants have been accomplished with either single-cell suspensions of established cell lines or direct surgical explants. Reports of xenotransplantation of horse tumors are limited to a sarcoid derived cell line<sup>28</sup> and an undifferentiated skin carcinoma.<sup>29</sup> Cell lines of equine SCC have not been established to date. Xenografts derived from cell lines generally show a homogeneous undifferentiated histology, due to selection of a cell population with repeated passages resulting in histologic changes from the original tumor.<sup>30</sup> In contrast, xenografts established by implantation of fresh tumor tissue sections have been shown to more closely resemble the original patient specimens in their architecture and morphology.<sup>31,32</sup>

### **3. TISSUE CRYOPRESERVATION**

In human medicine, there is a rapidly growing interest in “tumor banking”, where small pieces of frozen tissues are preserved for possible future ancillary studies. Cryopreserved specimens offer readily available samples to be utilized in exploring novel cancer treatment options, genetic assays, chemosensitive assays, and tumor cell vaccines.<sup>33,34</sup> Use of cryopreserved samples for xenotransplantation avoids the difficulties associated with cell cultures and continuous animal passage, including contamination, accidental loss, genetic mutation.

## **4. PHOTODYNAMIC THERAPY**

### **a. Overview**

Photodynamic therapy (PDT) is an evolving modality for the treatment of a variety of ailments, including solid tumors, age-related macular degeneration, and atherosclerotic plaques.<sup>35-38</sup> PDT involves the use of photochemical reactions mediated through the interaction of photosensitizing agents, light and oxygen.<sup>39,40</sup> Photosensitizers are typically given intravenously and are preferentially retained in neoplastic tissue.<sup>40</sup> Upon activation by visible light matching the drug's absorption spectrum, the excited photosensitizer reacts directly with organic substrates to produce free radicals or reacts with ground state triplet oxygen to generate singlet oxygen.<sup>39</sup> This photodynamic process causes irreversible oxidation of one or more critical cellular components including plasma membranes, mitochondria, and lysosomes, inducing necrosis and apoptosis of the treated tissue. PDT also induces oxidative damage to the microvasculature contributing to ischemic tumor death.<sup>40</sup> Because a photosensitizer is preferentially absorbed by proliferative abnormal tissue and the light source is directly targeted on the lesion, PDT achieves highly selective treatment of a target area while minimizing damage to adjacent, healthy structures. With the exception of transient cutaneous photosensitivity and some tissue swelling, PDT has no other known systemic toxic side effects and is not carcinogenic or mutagenic at the doses used clinically.<sup>41,42</sup>

### **b. Photochemistry of photodynamic therapy**

A photosensitizer has no effect on tissue unless it is activated by light of the appropriate wavelength. When the photosensitizer chromophore is illuminated with light

of the specific wavelength that matches the electronic absorption spectrum of the photosensitizer, it is excited to a singlet state. Once it has absorbed energy in the form of electromagnetic radiation, it can return to ground state by a number of pathways. The chromophore can relax back to the ground state, by emitting photons between the same spin states (fluorescence), or be converted to excited triplet states via internal conversion (IC) and intersystem crossing (ISC), which is a radiationless transition between different spin states during collisions with other molecules. This reaction is represented by the Jablonski diagram (**Figure 1**).<sup>39</sup>

In oxygenated environments the triplet excited state photosensitizer ( $^3P^*$ ) readily transfers its energy to ground state molecular oxygen  $^3O_2$  to produce singlet oxygen  $^1O_2$ . These interactions of photosensitizers with molecular oxygen are known as Type-II reactions. Once activated, an excited photosensitizer ( $^3P^*$ ) can also react directly with organic substrates (S) by electron exchange producing an oxidized substrate ( $S^+$ ) and reduced photosensitizer ( $P^-$ ). The excited photosensitizer ( $^3P^*$ ) can also react with superoxide radicals ( $O_2^-$ ) to produce superoxide anions ( $O_2^-$ ) which can then create the highly reactive hydroxyl radical (OH). These reactions are called Type-I photoreactions. Type II reactions are reported to dominate during PDT. However, Type-I reactions may become more dominant under conditions where photosensitizers are highly concentrated, and especially under hypoxic conditions.<sup>43</sup> Singlet oxygen and free radicals generated through photochemical reactions are toxic to cells and tissues.

### **c. Biological mechanisms of action**

Most photosensitizers localize to cytosolic targets such as Golgi, endoplasmic reticulum, mitochondria, lysosomes, and membranes.<sup>44-46</sup> Geze et al. suggested that

hydrolases and acid that leak out of the damaged lysosomes may degrade cellular components.<sup>47</sup> Photosensitizers that localize to lysosomes may also re-localize to more susceptible organelles such as the membranes of the mitochondria or nuclei after rupture of lysosomes.<sup>48</sup> Studies have shown that PDT results in inhibition of several mitochondrial proteins including malate dehydrogenase, succinate dehydrogenase, and cytochrome *c* oxidase.<sup>49</sup> These proteins are required to maintain the electrochemical gradient across the inner-mitochondrial membrane. Among these proteins, cytochrome *c* oxidase was inhibited to the greatest extent in one study.<sup>49</sup> Another proposed target of PDT includes a protein complex termed permeability transition pore (PT pore).<sup>50</sup> The complex consists of hexokinase, the peripheral benzodiazepine receptor, the voltage-dependent anion channel, creatine kinase, the adenine nucleotide translocator and cyclophyllin D.<sup>50</sup> As these permeability transition pores open in response to PDT, small molecules flow in and out of the mitochondrial matrix resulting in disruption of mitochondrial membrane potential and mitochondrial swelling.<sup>51</sup> This process also results in breakdown of uncoupling electron transport chain and release of detrimental reactive oxygen species inducing apoptosis.<sup>52,53</sup> Reduced activity of adenosine triphosphatase (ATPase) has also been demonstrated with PDT.<sup>54</sup> Damage to subcellular targets lead to rapid apoptosis and necrosis of tumor cells.

Vascular destruction is also considered to be an important mechanism of tumor death in vivo for most photosensitizers being investigated clinically. Microscopically, the tumor tissue is characterized by endothelial cell damage, platelet aggregation, vasoconstriction, and hemorrhage following PDT.<sup>55-57</sup> Damage to the vascular endothelial cells is believed to be associated with platelet activation and release of factors such as

eicosanoids, in particular thromboxane, histamines and tumor necrosis factor  $\alpha$ .<sup>57-59</sup> PDT may also lead to vessel constriction via inhibition of the production or release of nitric oxide by the endothelium.<sup>60</sup> Microvascular collapse and thrombus formation lead to severe and persistent post-PDT tumor hypoxia/anoxia and may contribute to long-term tumor control.<sup>57,61-64</sup>

A strong inflammatory reaction is also an important event in the mechanism of PDT-mediated tumor destruction. Photooxidative lesions of membrane lipids prompt accelerated phospholipid degradation with a massive release of lipid fragments and metabolites of arachidonic acid, which act as powerful inflammatory mediators.<sup>65</sup> Endothelial damage also leads to a massive release of various inflammatory mediators.<sup>66</sup> Potent inflammatory mediators released following PDT include vasoactive substances, components of the complement and clotting cascades, acute phase proteins, proteinases, peroxidases, radicals, leukocyte chemo-attractants, cytokines, growth factors and other immuno-regulators.<sup>66,67</sup> Among cytokines, IL-6 mRNA and protein were found to be strongly enhanced in PDT treated mouse tumors.<sup>68</sup> In response to the inflammatory signaling, large numbers of neutrophils, mast cells, and monocytes/macrophages invade the treated tissue during and after PDT.<sup>69</sup> Lysosomal enzymes and reactive oxygen species secreted by neutrophils destroy endothelia and tumor cells and further amplify the inflammatory response.<sup>65,70</sup> In addition, generation of immune memory cells sensitized to PDT-treated tumors is believed to contribute to long-term tumor control.<sup>40,71</sup>

#### **d. Photosensitizer localization**

The mechanisms by which photosensitizers preferentially accumulate in tumors are not fully understood. Properties that have been implicated in the selective uptake and retention of photosensitizers in tumors include a large interstitial space, leaky vasculature, compromised lymphatic drainage, high number of tumor-associated macrophages which ingest certain PS, increased number of low density lipoprotein receptors, large amounts of newly synthesized collagen, low tissue pH levels, and high lipid content.<sup>40,72-74</sup> When compared to normal surrounding tissue, acidic tumor pH increases lipophilicity and therefore cellular uptake of photosensitizers.<sup>75</sup> Intratumoral lipid binds lipophilic photosensitizers, and porphyrins have an affinity for newly formed collagen.<sup>76,77</sup> Internalization of photosensitizers by the LDL receptor mediated pathway has been demonstrated.<sup>78</sup> Tumor cells have higher numbers of LDL receptors on their surfaces, potentially associated with their higher requirement for cholesterol than normal cells to build membranes.<sup>79</sup> Several studies have achieved preferential photosensitizer release to tumor cells by associating the photosensitizers with low density lipoproteins and by increasing hydrophobicity by augmentation with liposome delivery systems.<sup>80-82</sup> However, other studies have shown that a degree of selectivity does not correlate with their hydrophobicity or their affinity for LDL, indicating that the LDL-receptor mediated pathway may not be the main route of internalization<sup>83,84</sup>

#### **e. Photosensitizers**

Porfimer sodium was the first photosensitizer to have received FDA approval for treatment of esophageal and endobroncheal cancer, and it is currently used to treat a wide



variety of cancers.<sup>85</sup> It is synthesized from hematoporphyrin and it is composed of monomers, dimers, trimers and larger oligomers.<sup>86</sup> Porfimer sodium has 2 major disadvantages. First, it results in prolonged skin photosensitivity lasting for 6 to 8 weeks.<sup>40</sup> Second, activation of porfimer sodium occurs at 630 nm, which limits the depth of light penetration in tissue to less than 5 mm.

Newer generations of photoactive agents are being developed with reduced risk of unwanted side-effects. Second generation photosensitizers include newer synthetic products of various groups (porphines, porphycenes, chlorines, phthalocyanines and others) that possess a better pharmacological profile, including more efficient light absorption and a higher quantum yield for singlet oxygen.<sup>87,88</sup> One such agent, verteporfin (Benzoporphyrin derivative monoacid A ring, BPD-MA, Visudyne®), synthesized from protoporphyrin, has been approved for the treatment of people with macular degeneration.<sup>89</sup> Verteporfin is a chlorin-type molecule derived from porphyrine and exists as an equal mixture of two regioisomers, BPD-MA<sub>C</sub> and BPD-MA<sub>D</sub>. Pharmacokinetic studies with intravenous injection showed a  $t_{1/2}$  of 5 to 6 hours with the drugs distributed particularly to the liver, spleen and kidneys.<sup>90</sup> Most of an injected dose of verteporfin is cleared within 24 hours in mice.<sup>91</sup> Due to its rapid plasma and tissue pharmacokinetics, verteporfin results in less skin photosensitivity than do first generation photoactive drugs.<sup>90,92</sup> In addition, verteporfin has an absorption maximum around 690 nm, and this wavelength permits activation of the drug within the deeper portions of the target tissue than older photoactive agents.

#### **f. Light source and delivery**

Lasers are most frequently used for PDT because of their highly coherent monochromatic light that can be channeled into quartz fibers used as light delivery devices. Light is usually delivered through fiber-optic cables to the treatment site. Diode lasers are becoming available, replacing the labor intensive argon pumped dye lasers. Non-coherent light sources, such as filtered lamps or light emitting diode (LED) arrays have also become available for PDT. These offer several advantages over a laser including lower equipment costs, minimal risk of personnel eye damage and no special electrical or plumbing requirements. Limitations of non-coherent light sources include low power output and difficulty in launching light into small optical fibers.<sup>93</sup>

The choice of photosensitizer dictates which wavelength of light is required for treatment. For example, porfimer sodium is activated at 630 nm, whereas verteporfin is activated at 690 nm. The depth of penetration of laser light depends on the light's wavelength, on whether the laser is superpulsed, and on the power output. Light in the 600-700 nm region of the spectrum penetrates 50-200% more than light in the 400-500 nm region.<sup>94</sup> Pogue et al evaluated average depth of tissue necrosis using BPD-MA with irradiation protocol of 50 J cm<sup>2</sup> and 200 mW, 690 nm continuous wave produced from an argon ion pumped dye laser delivered to a subcutaneous rat prostate model. The study showed an average penetration depth of 8.7 mm.<sup>95</sup> The penetration of the light is also very much dependent on the type of tissue involved. Highly pigmented tissues or tissue with high hemoglobin content, such as muscle, can reduce the depth that light can penetrate.<sup>96</sup>

## CHAPTER 2

### EXPERIMENTAL PURPOSE AND HYPOTHESIS

In PDT, a photosensitizer is typically administered to the patient by intravenous injection. However, intravenous injection of a photoactive drug to a horse is not feasible at this time. Pharmacokinetic, drug distribution, and toxicology studies have not been conducted using these agents in horses, and the amount of drug to be delivered would likely be excessive in volume and expense. Additionally, intravenous application of the drug can result in sunlight-induced skin photosensitization, requiring horses to remain indoors for up to several weeks. Stall confinement predisposes the equine patient to potentially life-threatening maladies including colic and respiratory infection. At the University of Missouri-Columbia, Veterinary Medical Teaching Hospital, we are investigating a novel approach to the treatment of equine periocular SCC. In equine patients undergoing local PDT, a photoactive agent is injected locally into the wound bed immediately after surgical resection of the tumor followed by light irradiation.<sup>97,98</sup>

A reproducible murine model is essential to prospectively investigate key basic science questions regarding the effectiveness of local PDT on SCC. Reports of xenotransplantation of equine tumors are limited to a sarcoid derived cell line and an undifferentiated skin carcinoma.<sup>28,29</sup> To date, a clinically relevant in vivo model for equine SCC does not exist. In study 1, we examined the ability to cryopreserve ocular SCC obtained from 3 affected equine patients and the ability of SCID and nude mice to support growth of cryopreserved tumor tissue. The morphological and histological

appearance and characteristic staining for cytokeratin 5/6 and p53 of the cryopreserved tissue sections and xenografts in mice were compared with these of the original host tumors.

In study 2, we developed a nude mouse model, bearing human skin origin SCC. Specifically, we report the use of intratumoral injection of verteporfin as a means of drug administration for PDT and the efficacy of local PDT on growth inhibition of SCC. Response rates with respect to drug dose and type of solvent were compared. We hypothesized that local PDT with verteporfin would result in growth inhibition of subcutaneous SCC in a murine model and that response rate would be drug dose dependent. Further, we hypothesized that use of dimethyl sulfoxide (DMSO) as a solvent would result in better treatment response rates than use of 5% dextrose solution in water (D5W) as a solvent.

## CHAPTER 3

### STUDY 1: DEVELOPMENT OF A MURINE MODEL FOR EQUINE OCULAR SQUAMOUS CELL CARCINOMA

#### MATERIALS AND METHODS

##### Animals:

SCID mice, Fox Chase Outbred female, 4-5 weeks of age, weighing 16 to 20 g, were obtained from Charles River Laboratory, MA, USA. Athymic nude mice, *Foxn 1<sup>nu</sup>* female, 4-5 weeks of age, weighing 16-20 g, were obtained from Harlan Sprague Dawley, IN, USA. Mice were kept in sterile microisolator cages with autoclaved bedding, placed in a laminar air-flow cabinet under specific pathogen-free conditions with a controlled temperature of 72 °F, humidity of 45% and 12-h light cycle. Animals were given autoclaved food and acidified water (pH 2.8) *ad libitum*. All manipulations were performed in a laminar flow hood under sterile conditions. Enrofloxacin (West Haven, CT) was supplemented in the drinking water (75mg/450 mLs) for 2 weeks following tumor implantation. All animals used in this study were handled in strict adherence to institutional Animal Care and Use Committee guidelines and to the ARVO Statement for the Use of Animals in Ophthalmic and Vision Research.

##### Tumor collection and cryopreservation:

Spontaneously occurring primary ocular SCC was surgically excised from 3 affected equine patients at the University of Missouri, College of Veterinary Medicine, Veterinary Medical Teaching Hospital (**Table 1**). Tumors in each horse were located in the 3<sup>rd</sup>

eyelid, cornea and conjunctiva, originally measuring 1 x 1 x 3 cm, 2.5 x 2 x 0.5 cm and 1.5 x 1.5 x 0.8 cm in diameter, respectively. Tumors were handled using sterile technique, and sections of each tumor were fixed in 10% sodium phosphate buffered formalin for histologic evaluation. Remaining tumor sections were cut into 1.5 mm<sup>3</sup> cubes and incubated in 10 ml of TL-Hepes buffer solution supplemented with BSA and 1.5 M dimethylsulfoxide (DMSO, Sigma, MO) for 30 minutes at room temperature.<sup>99</sup> The tissues and medium were then aspirated into a 0.5-mL freezing straw and cooled initially to -7 °C at a rate of 1 °C/ min in a programmable freezer (Planer, Model: Kryo 10 Series II). At -7 °C, ice crystallization was initiated by touching the side of the straws with a cotton-tipped swab that was soaked in liquid nitrogen. After a 5-min isothermal hold, the cooling rate was decreased to 0.5 °C/ min. Once the temperature reached - 55 °C, the straws were transferred to liquid nitrogen for storage until implantation.

#### Cell viability test:

Cryopreserved equine SCC tissues, stored in liquid nitrogen for approximately 1 year were prepared for transplantation by thawing at 20 °C and washing three times in sterile TL-Hepes solution. Cell viability of the frozen-thawed tissue sections was determined with use of ethidium homodimer-1 (13µL/mL) and calcein AM (0.4 µL/mL) fluorescent stains (Live/Dead Viability/Cytotoxicity Kit, Molecular Probes; Eugene, OR) and a confocal microscope (BioRad Radiance 2000 system coupled to an Olympus IX70 inverted microscope equipped with Krypton-Argon mixed lasers and a red diode laser). Approximately 1.5 mm thickness tumor cross-sections were incubated with the stains in phosphate buffered saline for 30 minutes at room temperature. The numbers of calcein

AM stained viable cells (green fluorescence) and ethidium homodimer-1 stained non-viable cells (red fluorescence) of all sections were objectively evaluated using image analysis software (Image-Pro Plus, MediaCybernetics; Carlsbad, CA). Remaining tissue sections were transferred to a stir flask at 37 °C with 0.2 % trypsin plus 0.2 % collagenase to disaggregate into single cells. Cell viability was also determined on cell suspensions with a Trypan blue dye exclusion test. An equal volume of cell suspension (100µL) and 0.4 % (w/v) Trypan blue were mixed and loaded onto a hemocytometer to count the cells. The proportion of viable cells was determined by comparing the number of non-viable cells stained blue by Trypan blue and viable cells which remained clear of the dye.

#### Transplantation of equine tumor:

Under general anesthesia with a continuous flow of 100% oxygen containing isoflurane, equine tumor sections from 3 horses measuring 1.5 mm in diameter were implanted into the dorsal lumbar subcutaneous tissues of the right flanks in 15 athymic nude mice and 15 SCID mice using a 3-mm microsurgical knife (Surgical Specialties Corp., PA). Five mice of each strain were randomized to receive tumor sections from each of the 3 original equine patients. Transplantation was performed within 20 minutes following thawing of the tissues. A “take” was defined as an increase in volume of the tumor compared to the original transplantation. Mice were evaluated daily, and tumor growth rates were calculated after measuring the size of the tumor in three dimensions using Jameson calipers. The tumor volume,  $V$ , was calculated using the formula  $V = (l \times w \times h) \times \pi/6$ , where  $l$  is the longest axis of the tumor,  $w$  is the axis perpendicular to  $l$ , and  $h$  is the height of the tumor. The mice were euthanized by cervical dislocation at day 150, and

tumor, lung, liver, kidney, spleen and regional lymph node tissue from xenografted mice were harvested and immediately processed as described below.

Histopathological examination:

Representative tumor sections from 3 original equine patients, cryopreserved tumor tissue and tumors from xenografted mice were each fixed in 10% sodium phosphate buffered formalin, paraffin embedded and stained with hematoxylin-eosin (H&E). Morphologic features were examined by a board-certified veterinary pathologist (J. Turk), using light microscopy. Additional tumor sections were processed for immunohistochemistry.

Briefly, tissues were cut at 4  $\mu\text{m}$  and placed on positively-charged slides. The slides were irradiated in a microwave oven (700 W) and left on a 43 °C slide warmer overnight.

They were hydrated in graded ethanol and steamed at 95 °C for 20 min in Citrate Buffer (DakoCytomation, Carpinteria, CA) pH 6.0, rinsed, and placed in Tris-buffered saline.

Slides were treated with 3%  $\text{H}_2\text{O}_2$  for 15 min, washed in buffer, treated with Protein Block (DakoCytomation, Carpinteria, CA) for 5 min and drained. Slides were then incubated in mouse anti-Cytokeratin 5/6 antibody (clone D5/16B4, Zymed, South San Francisco, CA) or rabbit anti-P53 antibody (SC-6243, Santa Cruz Biotechnology Inc., Santa Cruz, CA) for 60 min. Negative controls were treated with mouse IgG (Sigma, St. Louis, MO) for 60 min. Secondary and tertiary reagents used for cytokeratin stain were biotinylated anti-rabbit, anti-mouse and anti-goat immunoglobulins (LSAB2+.

DakoCytomation, Carpinteria, CA) and streptavidin conjugated to horseradish peroxidase (LSAB2+. DakoCytomation, Carpinteria, CA) for 20 min each. The chromogen used was DAB+ (DakoCytomation, Carpinteria, CA.) for 5 min. The secondary reagent used



for p53 stain was rabbit Envision+ (DakoCytomation, Carpinteria, CA) for 30 min. The chromogen used was Nova Red (Vector, Burlingame, CA) for 10 min. Slides were then counterstained in Mayer's Hematoxylin (Newcomer's Supply, Appleton, WI) for 1 minute, dehydrated and cover slipped. The stained sections were subjectively evaluated for the presence, intensity and location of staining. Lung, liver, kidney spleen and regional lymph node tissue from each mouse were evaluated histologically for evidence of metastases.

## **2. RESULTS**

### Cell viability

The effect of cryopreservation on cell viability in frozen-thawed tissue sections from 3 horses was evaluated with ethidium homodimer-1 and calcein AM fluorescent stains (**Figure 2**). The mean percentage ( $\pm$  SD) of viable cells indicated by green fluorescence for each sample was 63.3 ( $\pm$  8.8) %. Non-viable cells were sparsely interspersed among live cells with more non-viable cells noted at the periphery of each tissue section. The mean percentage ( $\pm$  SD) of viable cells in cell suspension determined by Trypan blue dye exclusion test was 61.5 ( $\pm$  4.1) %.

### Tumor implantation efficiency and growth rate

Tumor growth was observed in 1 recipient SCID mouse (**Figure 3**) and 2 nude mice. The tumors were well circumscribed solid masses located in the subcutaneous space of each mouse. The latent period between subcutaneous implantation and the first evidence of tumor growth ranged between 27 and 29 days. The tumor reached 2010 mm<sup>3</sup> in a

SCID mouse at day 150. The tumors in the nude mice were 1590 mm<sup>3</sup> and 879 mm<sup>3</sup> at day 150. Tumor doubling time ranged from 5 days (at day 30) to 35 days (at day 90), with slower growth rate observed with time (**Figure 4**). Mean tumor doubling time was 14.5 days.

#### Histopathologic evaluation

Histopathologic examination was performed on original equine tumors, cryopreserved tumors, and xenografted tumors (**Figure 5**). The cut surfaces of the xenografted tumors were homogenous grayish-white with focal, yellow, central necrotic areas. All xenografted tumors were well-circumscribed with distinct fibrous capsules and were restricted to the subcutaneous space. Histopathologic evaluation of xenografted tumors confirmed well differentiated SCC with multifocal dyskeratosis, keratin pearls, and 1-3 mitotic figures per 400x field. There were no marked morphologic differences between the primary equine tumors, cryopreserved tumors and xenografted tumors. Characteristic diffuse and strong positive immunoreactivity for cytokeratin 5/6 remained the same in its intensity and location after cryopreservation and transplantation (**Figure 5**).

Immunoreactivity for p53 appeared as a dark brownish granular signal and was found solely in the nucleus, predominantly in the periphery of the neoplastic islands with loss of staining toward the keratinized center in excised (**Figure 6A**), cryopreserved (**Figure 6B**), and transplanted (**Figure 6C**) ocular SCC. In all cases, tumors demonstrated only local growth without evidence of invasion into lymphatics or blood vessels. There was no evidence of metastases by visual inspection at the time of necropsy or by

histopathological examination of lung, liver, kidney, spleen and regional lymph node tissue.

### **3. DISCUSSION**

Tumor xenografts have been widely used in human medical research using both nude and SCID mice. The absence of functioning cell mediated immunity (T cells) in nude mice can permit the growth of xenotransplanted tumor tissues without subsequent rejection. SCID mice lack both functional T and B lymphocytes, eliminating much of the compatibility issues associated with host immunity.<sup>100</sup> Both athymic nude and SCID mice were used as recipients in the present study. The primary tumor take rate of equine SCC for nude and SCID mice was 13% and 7% respectively. This is compatible with previous reports discussing the difficulty in establishing SCC in nude mice.<sup>101,102</sup> Previously reported take rates of fresh SCC xenografts were 0% for canine SCC transplanted in SCID mice<sup>103</sup>, 72% for ovine SCC transplanted in athymic nude mice<sup>27</sup> and 50% and 25.9% for human SCC transplanted into SCID and nude mice, respectively.<sup>104, 105</sup> The tumor xenografts in the present study showed a latent period of 27 to 29 days followed by progressive growth with tumor doubling time ranging between 5 days (at day 30) to 35 days (at day 90). Although these tumors did not display a typical Gompertzian growth pattern with sigmoid-shaped growth curves, slower growth rates were observed at the later stages of the study. It is possible the tumors would have reached their Gompertzian plateau phase if the tumors were allowed to grow longer than 150 days.

Reported take rates for tumors vary depending on several factors. The location of inoculation impacts take rate with subcutaneous tissue demonstrating a lower take rate

compared to intravenous, intracranial, and intraperitoneal implantation.<sup>106</sup> Influence of the inoculation site was also demonstrated in breast tumors where the tumor could not be successfully transplanted to the subcutaneous tissue of nude mice but grew readily when transplanted to the mammary fat pad.<sup>107</sup> A subcutaneous space was chosen as an implantation site for this study because the original tumor was a cutaneous carcinoma, and this location provided the most similar microenvironment for the xenotransplanted tumors to grow. In addition, subcutaneous tumors are easily accessible for inspection and local treatment, and their response to treatment can easily be measured. As solid cryopreserved tissue sections were used as the tumor source in the present study, subdermal implantation would have been difficult to perform. A dissociated cell suspension was considered for use in this study, with subdermal or subcutaneous implantation as a means of optimizing vascularization.<sup>32</sup> However, this procedure was not performed because xenografts derived from cell suspension carry a greater risk of not accurately reproducing the biologic and histopathologic characteristics of the original tumor.<sup>30</sup>

The ability to successfully transplant tumors also relates to inherent differences in the tumor cells themselves and the number of cells implanted.<sup>27,108</sup> In general, the take rate correlates closely with the invasiveness and metastatic capability of the tumor.<sup>106</sup> Braakhuis et al. (1984) showed higher take rates in poorly differentiated human head and neck SCC than moderately and well-differentiated SCC, suggesting that higher proportions of stem cells and viable cells present in poorly differentiated SCC may better support tumor growth.<sup>104</sup> All equine ocular SCC used as tumor sources in this study were confirmed to be well-differentiated tumors by histopathology. In general, equine ocular

SCC demonstrates a relatively slow growth rate and a low metastatic rate compared to some other equine tumors. The relatively low take rate in the current study may reflect a low growth potential inherent to this tumor type in mice.

Successful growth of various xenotransplanted tumors has been reported with inoculation of  $5 \times 10^4$  to  $1 \times 10^6$  tumor cells.<sup>108</sup> In the present study, a minimum of  $2 \times 10^5$  viable cells were considered to be present in each implanted tissue section based on the size of the tissue and the results of viability tests. Kopf-Maier et al. (1986) described necrosis of the majority of the colon adenocarcinoma cells shortly after xenotransplantation, before regeneration and proliferation of tumor cells can occur.<sup>109</sup> The number of transplanted cells in the present study may have been insufficient to assure tumor growth in all mice due to cell death in the initial stage immediately following transplantation.

Regeneration and proliferation of xenotransplanted tumor cells occur only after host connective tissue invades the implants; connective tissue serves as a ground substance and guides the development of blood vessels which supply required nutrients.<sup>109</sup> The low take rate in this pilot study may have been associated with inadequate production of extracellular matrix or insufficient chemical signals secreted by the host stromal cells including angiogenic factors and soluble growth factors. Based on the importance of host stromal cells for tumor growth, injection of cultured fibroblasts along with different types of tumor cells has been attempted.<sup>110,111</sup> In these studies, a significant stimulating effect of the fibroblasts on the tumor take rate was observed when the number of tumor cells was below the tumorigenic dose. Addition of radiation-killed tumor cells or a brain-tissue brei at the time of inoculation has also been shown to

improve the take rate and growth rate in cases of small viable inoculum or less aggressive tumor type.<sup>110,112</sup> Tumor growth is believed to be promoted by this “feeder-layer effect” due to secretion of angiogenic and growth factors. Use of such feeder cells may be required to improve the take rate for equine ocular SCC in a murine model.

The cytotoxic immune response of the host is an important factor in tumor rejection.<sup>113</sup> Although nude mice lack mature T lymphocytes, other types of cell-mediated immune responses, such as B cell antibody response, are present.<sup>114</sup> Mice with immune defects in the function of B cells, NK cells or both, such as SCID mice, are generally better hosts in some cases for xenotransplants than nude mice. The growth of xenotransplanted tumors in athymic nude mice is less predictable compared to SCID mice.<sup>115</sup> In some human tumors, xenografts subcutaneously transplanted into SCID mice grow more rapidly, developing larger tumors compared to athymic nude mice.<sup>113,116</sup> In the present study, no apparent difference in tumor take rate, latent period or growth rates were observed between nude and SCID mice. Based on these findings, the residual immune system of the nude mice does not appear to substantially contribute to the relatively low take rate observed.

The establishment of skin SCC cell lines has been limited by the low success rate of *in vitro* culture.<sup>117,118</sup> Although successful culture of normal equine keratinocytes has been reported, an equine SCC cell line has not been established to date.<sup>119</sup> Human SCC cell lines vary in their requirement for a fibroblast feeder layer such as mouse 3T3 cells, collagen scaffold, growth factors and hormones to support clonal growth,<sup>120,121</sup> and alteration in the degree of differentiation in neoplastic keratinocytes under different culture conditions has been reported.<sup>122,123</sup> In addition, cell lines bear the risk of

phenotypic change, taking up foreign DNA and developing mutations in the p53 gene.<sup>118,121,124</sup> With successful cryopreservation, tumor tissues can be thawed and implanted on an as-needed basis for development of a tumor model. Transplantable frozen samples provide a readily available tumor source without the need for repeated harvesting procedures, continuous animal passage or cell culture. In addition, xenotransplantation of cryopreserved tissue avoids the risks of biological and chemical contamination that have been associated with tissue culture. Furthermore, cryopreserved tissues or cell banks could provide sufficient numbers and varieties of tumor types to be useful in oncology research.

No prior scientific study on the cryopreservation of equine SCC has been reported. Comparison of cell survival calculations between those obtained from ethidium homodimer-1 and calcein AM fluorescent stains vs. Trypan blue dye exclusion test revealed that the assay results were highly correlated. Over 60% of the cells were viable after cryopreservation in our study, which is similar to another study in which 50 to 60% post-thaw survival was reported with normal human epidermal keratinocytes.<sup>125,126</sup> In addition to necrosis immediately subsequent to the freezing and thawing process, cryopreservation-induced delayed-onset cell death (CIDOCD)<sup>127</sup> and arrest of cell division and function have been recently demonstrated.<sup>128,129</sup> These reports described cell death over a period of up to 24 hours following cryopreservation, indicating that the cell survival rates may be overestimated with short-term post-thaw assessment. The viability tests in the present study were performed within 1 hr of thawing and were designed primarily to detect damage of the plasma membranes and the enzymatic activity of

cytosolic esterase. Assessment of survival over the initial 24 hours of thawing may reveal a contribution of CIDOCD and is warranted.

The histological appearance of the xenografted SCC was in full accord with the original equine tumors with preservation of characteristic immunohistochemical cytokeratin 5/6 staining. Previous studies showed overexpression of p53 in equine periocular SCC suggesting that UV radiation-induced p53 mutation may be one of the important factors involved in the pathogenesis of periocular SCC.<sup>130</sup> In moderately differentiated equine ocular SCC, positive staining reactivity involved most of the tumor cells' nuclei.<sup>131</sup> In the present study, similar to previous reports in horses and cattle with well-differentiated SCC, positive immunoreactivity was found solely in the nucleus and predominantly in the periphery of the neoplastic islands with loss of staining toward the keratinized center in excised, cryopreserved, and transplanted ocular SCC.<sup>131,132</sup> Expression of p53 protein was not detected in normal tissues. These findings suggest that any alteration in phenotype or cell differentiation was minimal following cryopreservation and xenotransplantation, further supporting these methods as useful tools in creating a murine model for equine ocular SCC.

Most studies using a murine tumor model have focused on the effects of various new therapeutic agents or treatment modalities for the particular tumor type. Studies have shown that tumor xenografts in murine models demonstrate clinically relevant response rates to various treatments.<sup>16</sup> Human bronchial carcinoma xenografts reproduce the chemotherapeutic response pattern of their source tumors and thus play an important role in the investigation of new chemotherapy agents.<sup>133</sup> Equine SCC established with transplantation of cryopreserved tissue in the present study maintained and reproduced



the original cellular morphology and differentiation indicating that this model may be a relevant *in vivo* system for studying the biology of this important tumor type in veterinary ophthalmology. This model has potential to be used as a preclinical screen for new therapeutic agents and treatment modalities for equine ocular SCC. The low take rate observed in the present study may be improved with modification of cryopreservation methods, use of fresh tissue samples, or transplantation with feeder cells.

## CHAPTER 4

### STUDY 2: LOCAL PHOTODYNAMIC THERAPY FOR SQUAMOUS CELL CARCINOMA IN A MURINE MODEL

#### MATERIALS AND METHODS

##### Animals

All animals used in this study were handled in adherence to institutional Animal Care and Use Committee guidelines. Athymic nude mice *Foxn1<sup>nu</sup>* (Harlan Sprague Dawley, Indianapolis, IN), female, 6 to 8 weeks old, were kept in sterile microisolator cages with autoclaved bedding, placed in a laminar air-flow cabinet under specific pathogen-free conditions with a controlled temperature of 72 °F, humidity of 45% and 12-hr light cycle. Animals were given autoclaved food and acidified water *ad libitum*. All manipulations were performed in a laminar flow hood under strict sterile conditions.

##### Tumor Model

A-431 human epidermoid SCC cells (American Type Culture Collection, Manassas, VA) were maintained in a humidified 5% CO<sub>2</sub> atmosphere at 37 °C, using Dulbecco's modified Eagle medium (American Type Culture Collection, Manassas, VA) supplemented with 10% fetal bovine serum (American Type Culture Collection, Manassas, VA) and 1% penicillin-streptomycin solution (American Type Culture Collection, Manassas, VA). Upon reaching confluence, cells were trypsinized with 0.25% trypsin-ethylenediamine tetraacetic acid (Sigma Chemical Co, St Louis, MO). To

accomplish xenografting,  $5 \times 10^6$  A-431 cells were suspended in 0.1 mL of Dulbecco's phosphate-buffered saline and injected into the dorsal lumbar subcutaneous space of each mouse using a 27-gauge hypodermic needle on a tuberculin syringe. Mice were monitored daily and tumor size was assessed by taking three caliper measurements at right angles to each other. Tumor volume was derived by applying the following formula, considering the tumor as a hemiellipsoidal mass:  $\text{volume (mm}^3\text{)} = \pi/6 (l \times w \times h)$ ; where  $l$  = length,  $w$  = width, and  $h$  = height in millimeters.<sup>134</sup> Experiments were initiated once tumor volume reached a minimum of 150 mm<sup>3</sup>. Average tumor size at the time of local PDT was 231 (+/- 59) mm<sup>3</sup>.

### **Photosensitizer**

Verteporfin for injection (Visudyne<sup>®</sup>, Quadra Logic Technologies, Inc., Vancouver, BC, Canada) was diluted in sterile water at 2 mg/mL and was further diluted with either dimethyl sulfoxide (DMSO) or 5% dextrose in water (D5W) to concentrations of 2 mg/mL, 0.2 mg/mL and 0.02 mg/mL. All concentrations were protected from light and were used within 4 hours of preparation.

### **Light delivery device**

Red light at a wavelength of 688 nm +/- 10 nm was delivered by a light emitting diode (LED, Quantum Devices Inc, Barneveld, WI). Irradiance was set at 100 J/cm<sup>2</sup> with a fluence rate of 200 mW/cm<sup>2</sup> for all experiments (duration of delivery per mouse: 8.3 minutes). Emission spot size was adjusted using different size stainless steel attachments on the LED, in order to minimize illumination of normal tissues around each tumor.

## **Experimental protocol**

Mice were anesthetized using a face mask and non-rebreathing system connected to an anesthetic machine that delivered isoflurane in oxygen. Mice were placed on a heated blanket maintained at 37 °C throughout the treatment. Verteporfin was injected locally into each tumor at a single site using a tuberculin syringe with a 27 G hypodermic needle. Tumors were illuminated with red light 5 min after verteporfin administration (**Figure 7**).

### **Experiment A: Drug dose evaluation**

In experiment A, the effect of drug dose was evaluated. Tumor bearing mice were randomly divided into 5 groups with 10 mice in each group (**Table 2**). Treatment group **A1** received a dose of 0.01 mg/cm<sup>3</sup> tumor volume at concentration of 0.02 mg/mL verteporfin in DMSO (0.5 mL/cm<sup>3</sup> tumor volume). Treatment group **A2** received a dose of 0.1 mg/cm<sup>3</sup> tumor volume at concentration of 0.2 mg/mL verteporfin in DMSO (0.5 mL/cm<sup>3</sup> tumor volume). Treatment group **A3** received a dose of 1.0 mg/cm<sup>3</sup> tumor volume at concentration of 2.0 mg/mL verteporfin in DMSO (0.5 mL/cm<sup>3</sup> tumor volume). Control groups **A4** and **A5** received DMSO alone, or light alone respectively. An additional control group **A6** (n = 5) received subcutaneous injections of 200 mg verteporfin in DMSO without light illumination to investigate toxic effects from the photoactive drug alone. This dose is compatible with 1.0 mg/cm<sup>3</sup> dose for an average size tumor (200 mm<sup>3</sup>). Mice in control group A6 were euthanized 24 hours after injection for necropsy.

## **Experiment B: Solvent evaluation**

In experiment B, the effect of solvent was evaluated. Tumor bearing animals were randomly divided into 4 groups with 10 mice in each group (**Table 3**). Treatment groups **B1** and **B2** received verteporfin at dose of 0.1 mg/cm<sup>3</sup> diluted in D5W and DMSO, respectively. The drug dose was determined based on results on Experiment A. Control groups **B3** and **B4** received D5W alone or DMSO alone, respectively. All mice were exposed to light as previously described.

### **Evaluation of tumor response**

All mice were monitored daily for overall body condition including appetite, hydration status and activity level. Body weight was measured twice weekly and all tumors were measured in 3 dimensions twice weekly to derive tumor volume. Tumors were observed for color change, edema and ulceration. Mice were euthanized 30 days after the time of treatment or when the tumor volume reached 1500 mm<sup>3</sup>. Necropsy and histopathology were performed on mice that died prior to the study end point in group A3 to evaluate the cause of death and on mice in group A6 to investigate toxic effects from the drug alone.

### **Statistical analysis**

The main outcome variable used in data analysis was the relative change in the tumor volume (RCTV) following treatment. This was derived by using the calculation  $(V_t - V_o)/V_o$ , where  $V_t$  represents the tumor volume at each measured time point, and  $V_o$  represents the tumor volume on day 0 (treatment). This allowed comparison of treatment efficacy between tumors regardless of differences in original tumor volume. Analyses

were performed using Wilcoxon Rank Sum test to compare mean RCTV between groups at day 13 and 30. A p value < 0.05 was considered statistically significant.

## 2. RESULTS

### **Local and systemic toxicity**

All tumors receiving any intratumoral injection developed mild edema extending approximately 3 mm into the surrounding tissue and lasting for less than 24 hr. Those tumors receiving verteporfin injection developed a dark green discoloration of the tumor which lasted 24-48 hr. Eschar formation followed by full thickness ulcers developed in tumors following PDT in 1 mouse in the treatment group A1, 4 mice in the treatment group A2 and 5 mice in the treatment group B1 (**Figure 8**). All ulcers were noted between 3 and 7 days post-treatment. Presence of skin ulceration did not adversely affect the overall health of mice as assessed by weight gain, appetite and activity level. Nine out of 10 mice in the group receiving  $1.0 \text{ mg/cm}^3$  verteporfin died within 1 hour following light illumination. Control animals treated with DMSO or D5W without verteporfin injection or light alone showed no significant local phototoxic effect. No systemic adverse effects were noted in other treatment or control groups receiving subcutaneous injections of 200 mg verteporfin without light illumination.

### **The effect of drug dose (Experiment A)**

Tumor volumes over the study period in experiment A are depicted in **figure 9**. Mean relative change in tumor volume (RCTV) for each group in experiment A at day 13 and 30 are shown in **figures 11 and 12**. No data for treatment group A3 were available

for analysis, due to loss of 9/10 mice shortly after the treatment. For mice that survived the peri-treatment period, local PDT of tumors resulted in significant alterations in tumor growth and size at day 13 and 30. By day 13, low dose verteporfin treatment (A1: mean RCTV = 1.381 +/- 0.741) significantly inhibited tumor growth as compared to the control group A5 (mean RCTV = 3.058 +/- 1.187), but not compared to the control group A4 (mean RCTV = 1.512 +/- 1.165) with p values of 0.005 and 0.739, respectively. The moderate dose verteporfin treatment (A2: mean RCTV = -0.118 +/- 0.74) resulted in significant reduction of tumor growth compared to both control groups A4 (p = 0.0006) and A5 (p = 0.0007). Additionally, mice in the moderate dose treatment group A2 had a significantly reduced RCTV compared to the low dose treatment group A1 (p=0.0003). By day 30, there was no statistically significant difference in mean RCTV between low dose treatment group A1 (mean RCTV = 4.228 +/- 2.049) and either control group A4 (mean RCTV = 6.231 +/- 5.454) or A5 (mean RCTV = 7.384 +/- 3.449) with p values of 0.429 and 0.032, respectively. Mean RCTV was significantly smaller in the moderate dose treatment group A2 (mean RCTV=1.642 +/- 2.47) compared to both control groups A4 and A5, with p values of 0.005 and 0.004, respectively. Again at day 30, mice in the moderate dose treatment group A2 had a significantly reduced RCTV compared to the low dose treatment group A1 (p=0.009).

The five mice treated with verteporfin and no light (A6) and five of nine mice that died acutely after local PDT in high dose treatment group A3 underwent necropsy examination. Segmental jejunal mucosal and serosal hemorrhage and meningeal hemorrhage were observed on gross necropsy in 3 mice in treatment group A3. Histologic examination of liver, kidney, lung, spleen and brain revealed that all mice in

treatment group A3, but none in control group A6, had multiple fibrin clots within the pulmonary vasculature. Congestion and hemorrhage within the GI tract, brain parenchyma and cerebral ventricular system were observed in mice in treatment group A3 but not in those of control group A6.

### **The effects of drug solvent (Experiment B)**

Tumor volumes over the study period in experiment B are depicted in **figure 10**. Mean relative change in tumor volume for each group in experiment B at day 13 and 30 are shown in **figures 13 and 14**. By day 13, treatment with verteporfin in D5W (B1: mean RCTV =  $-0.271 \pm 0.677$ ) significantly inhibited tumor growth as compared to the control group B3 (mean RCTV =  $0.618 \pm 1.107$ ) with p value of 0.049. Treatment with verteporfin in DMSO (B2: mean RCTV =  $-0.258 \pm 0.74$ ) resulted in significant reduction of tumor growth compared to the control group B4 (mean RCTV =  $1.512 \pm 1.165$ ) with p value of 0.0006. By day 30, there was no statistical difference in RCTV between D5W treatment group B1 (mean RCTV =  $2.326 \pm 3.746$ ) and D5W control group B3 (mean RCTV =  $4.128 \pm 8.404$ ) ( $p = 0.4179$ ). Statistically significant inhibition of tumor growth persisted in the DMSO treatment group B2 (mean RCTV =  $1.538 \pm 2.47$ ) compared to DMSO control group B4 (mean RCTV =  $6.231 \pm 5.454$ ) with p value of 0.0053. There was no statistical difference in mean RCTV between group B1 and B2 at both day 13 and 30 with p values of 0.396 and 0.561, respectively.

Complete tumor remission was achieved in 2 mice in treatment group B2 (**Figure 15**). Tumor volumes at the time of treatment for these mice were  $307.72 \text{ mm}^3$  and  $234.45 \text{ mm}^3$ , respectively (average size of original tumors for treatment group =  $195.28 \text{ mm}^3$ ).



The time at which complete tumor remissions occurred was 20 and 30 days post-treatment respectively. At the light dose used in this experiment, no significant local phototoxic effects were noted in groups that did not receive verteporfin or solvent.

### 3. DISCUSSION

Verteporfin is a chlorine-type second generation photosensitizer, now approved in many countries for the treatment of age-related macular degeneration. Second generation drugs possess a better pharmacological profile than the first generation drugs, including more efficient light absorption and a higher quantum yield for singlet oxygen.<sup>87,88</sup> Verteporfin was chosen as the photoactive agent in the present study, due to its desirable properties including a short photosensitivity period of only a few days, and a strong absorption peak at 688 nm, giving better depth of light penetration in tissue.<sup>135</sup> The reported PDT protocol with verteporfin in people and animals consists of systemic administration of verteporfin at doses of 0.5 to 2.0 mg/kg body weight, followed by exposure of target lesions to 40 to 150 J/cm<sup>2</sup> of photoradiation at 690 nm.<sup>92,136,137</sup> A complete clinical response rate of 95% has been reported in nonmelanoma skin cancers, including SCC in people treated with PDT using verteporfin administered intravenously with a drug dose of 0.6 mg/kg and a light dose of 180 J/cm<sup>2</sup>.<sup>92</sup> Local PDT entailing intratumoral injection of photoactive agents reported in subcutaneously implanted mouse glioma and mammary adenocarcinoma using a hematoporphyrin derivative suggested that selectivity and efficiency of PDT may be enhanced with local administration of photosensitizers.<sup>138,139</sup>

The present study demonstrates that local photodynamic therapy with verteporfin at dose of  $0.1 \text{ mg/cm}^3$  tumor volume effectively inhibited the growth of subcutaneous SCC in a murine model. No significant effect on tumor growth occurred in animals that received solvent alone or light alone. Verteporfin administered locally at a dose of  $0.1 \text{ mg/cm}^3$  tumor volume in our murine model attained equivalent body weight doses of 0.5 to  $1.0 \text{ mg/kg}$ .<sup>92,136,140,141</sup> This dose was compatible with previously reported successful treatment of SCC in humans with systemic administration of verteporfin.<sup>92,136,138</sup> In one murine model of mammary adenocarcinoma, intratumoral injection of porfimer sodium has been reported to result in 15 times higher porphyrin levels in tumor and 10 times greater rate of tumor mitochondrial enzyme inhibition compared to systemic injection, suggesting that local PDT may require a lower total dose of drug per patient.<sup>138</sup> However, in the current study, local PDT using the lower dose of verteporfin ( $0.01 \text{ mg/cm}^3$ ) was not shown to be effective in inhibiting the growth of SCC. This may be due to inadequate vascular effects elicited by local injection of the photosensitizer or presence of DMSO in the solvent preventing pathologies elicited by free radicals and reactive oxygen species.<sup>142</sup> Other factors that have also been reported to influence the response to PDT and chemotherapy include cellular glutathione S transferases and glutathione protecting cells from reactive free radicals.<sup>142,143</sup>

Local PDT with verteporfin at dose of  $1.0 \text{ mg/cm}^3$  resulted in significant mortality in our murine model; thus, dose effects on tumor growth inhibition could not be determined. Although no morbidity has ever been reported in people, severe cardiovascular complication and acute lethality following PDT have been documented in other species, including mice and cats.<sup>144,145</sup> In that report, the histological findings were

consistent with a systemic shock reaction; release of endogenous vasoactive mediators was speculated to be the likely cause of death.<sup>144</sup> Histopathology of the mice that died shortly after receiving our highest drug dose in the present study revealed multi-organ congestion and hemorrhage within gastrointestinal tract, brain parenchyma and cerebral ventricular system in conjunction with pulmonary fibrin clots, suggestive of disseminated intravascular coagulopathy (DIC). The relationship of PDT treatment area to total body area has been suggested as an important parameter in the induction of acute lethality in murine models. In the current study, the average tumor area was 68.1 mm<sup>2</sup> (approximately 10% of the average mouse body surface area) for the group that received high dose verteporfin (1.0 mg/cm<sup>3</sup>). Although a large tumor occupying as much as 10 % of the total body surface area in any species is unlikely to be treated with PDT alone, acute destruction of tissue mass of this size can potentially result in systemic shock reaction or DIC and should be considered. None of the mice that received verteporfin at a dose of 1.0 mg/cm<sup>3</sup> without light illumination developed any signs of systemic toxicity, suggesting that the high lethality in the 1.0/cm<sup>3</sup> dose group was likely associated with a PDT reaction rather than a response to the verteporfin itself.

Singlet oxygen has a short radius of action (10-20 μm), therefore, complete and homogenous distribution of the photosensitizer in the tumor is essential for effective tumor destruction with local PDT.<sup>40</sup> Studies have demonstrated that porfimer sodium, injected directly into the center of the subcutaneous glioma and bladder tumors, was retained and distributed throughout the entire tumor.<sup>139,146</sup> In addition, intratumoral administration yielded a much higher level of photosensitizer in tumor tissues and lower levels in normal tissues including the skin and other organs.<sup>147</sup> In the present study,

DMSO was compared to D5W as a solvent for verteporfin. DMSO is readily permeable to biological barriers including mucous membranes, cell and organelle membranes, and is widely used in veterinary medicine as an agent that enhances drug absorption across the skin.<sup>148-150</sup> We hypothesized that DMSO would increase local diffusion of verteporfin into solid SCC tumors, therefore resulting in better tumor growth inhibition. The final DMSO concentration used in the present study was 85.6%, which was considered to be sufficient to provide effective drug penetration based on previous studies.<sup>150-152</sup> However, there was no statistically significant difference in mean RCTV at a dose of 0.1 mg/cm<sup>3</sup> dose groups using DMSO or D5W.

Complete tumor regression was obtained in 2 mice that received verteporfin at a dose of 0.1 mg/cm<sup>3</sup> dissolved in DMSO. Interindividual variability in response rates observed in the current study may be associated with inconsistent and incomplete diffusion of the drug within the tumor. Longer time periods between injection and light illumination may allow better distribution of the photoactive agent and improve tumor destruction. Further investigation is warranted to identify the effect of DMSO on photosensitizer distribution and cellular localization as a function of time following local injection to determine the ideal drug-light interval. Other important properties of DMSO include its free radical scavenging capabilities and anti-inflammatory effects.<sup>148,150</sup> DMSO may have protected treated cells via detoxification of cytotoxic species, masking the potential beneficial effects of DMSO in drug distribution.

One of the primary factors that affect the efficacy of PDT is the depth of tumor from the incident surface of light illumination. The light wavelength required for PDT is dictated by the type of photosensitizer, and tissue penetration of light is directly

proportional to its wavelength.<sup>153</sup> PDT using porfimer sodium and a 630 nm laser at irradiation doses of 50 and 200 J/cm<sup>2</sup> has been reported to induce anti-tumor activity to a depth of 4.1 to 9.4 mm, respectively.<sup>154</sup> Therefore, we speculated that PDT using verteporfin and 690 nm light irradiation at 100 J/cm<sup>2</sup> might induce anti-tumor activity to a depth of more than 10 mm. The height of all tumors in the present study prior to the treatment was less than 10 mm. However, light transmission through living tissue is complex, influenced by tissue heterogeneity, stromal tissue density, tissue oxygenation and necrosis.<sup>155</sup> Relatively high stromal tissue density of SCC may have reduced the light penetration, leading to incomplete destruction of larger tumors. Two tumors that completely regressed in the present study had tumor volume of 307.72 mm<sup>3</sup> and 234.45 mm<sup>3</sup>. These tumors were larger than the average tumor size, suggesting that tumor volume may not be a major factor in treatment efficacy when treating small tumors less than 10mm in diameter. For larger equine periocular tumors, use of interstitial irradiation or surgical debulking prior to local PDT should provide adequate light penetration and more favorable long term prognosis.

Light dose and fluence rate also influence the efficacy of PDT. Light dose refers to the amount of light delivered to a given area and fluence rate refers to the rate of delivery. In a fibrosarcoma murine model and in cats with cutaneous SCC treated with PDT, depth of tumor necrosis and therapeutic outcome were found to be logarithmically proportional to increasing light energy delivered per unit area.<sup>156,157</sup> Synergistic enhancement of PDT by hyperthermia, associated with higher fluence rates, was suggested as the potential cause of improved therapeutic outcomes.<sup>157</sup> However, higher fluence rates may also lead to photochemical depletion of ambient tumor oxygen in some

cases, thus causing acute hypoxia and limiting treatment effectiveness.<sup>158</sup> In a murine fibrosarcoma model, PDT with light dose of 100 J/cm<sup>2</sup> at fluence rate of 30 mW/cm<sup>2</sup> resulted in significantly longer median tumor remission rates than PDT at 100 J/cm<sup>2</sup> and 150 mW/cm<sup>2</sup> demonstrating that in some cases, lower fluence rate can improve PDT response.<sup>158</sup> Light dose used in the current study was 100 J/cm<sup>2</sup> and fluence rate was 200 mW/cm<sup>2</sup> (total delivery time = 8.3 minutes). A higher light dose and lower fluence rate might have resulted in additional tumor growth inhibition and potentially better complete tumor regression rates.

A LED used as a light source in the present study generates less coherent light than a laser, but has a fairly narrow bandwidth. A LED offers several advantages over a laser including lower equipment costs, minimal risk of personnel eye damage and no special electrical or plumbing requirements. In addition, the LED probe does not require a fiber optic, which can create a substantial loss of power between the laser light source and the target tissue for light delivery. Successful application of PDT with a LED has been described for SCC in cats and humans.<sup>159,160</sup> Although a direct comparison between LED and laser cannot be made in this study, our results suggest that using a LED light source can be useful in local PDT for SCC, representing a cost-effective alternative to medical lasers.

A human SCC nude mouse xenograft was used as an equine tumor model in the present study. To date, a commercially available equine SCC cell line does not exist. We have previously reported on the development of equine ocular SCC by xenotransplantation of cryopreserved equine tumor sections.<sup>161</sup> These equine xenografted tumors maintained and reproduced their original cellular morphology and differentiation,

indicating the model may be a relevant *in vivo* system for studying the biology of this tumor type. However, the low take rate of that tumor model limited its use in the present studies. There may be differences in drug diffusion, absorption and overall effect of local PDT in other species affected by SCC, due to potential difference in immune responses elicited by PDT, and in glutathione level, vascularity, tumor pH, LDL and benzodiazepine receptor number in the tumor.

This study documents the first report of epidermal SCC treated with local PDT in a murine model. Results indicate that SCC can be effectively inhibited by local PDT. While our follow-up periods are relatively short, results obtained from this study indicate that tumor growth of SCC can be effectively inhibited using intratumoral injection of verteporfin. Additional studies are currently underway, examining differences in light dose and treatment response rates. Local PDT combined with surgical debulking has the potential of being used as a curative modality in horses affected by localized cutaneous SCC.

## TABLES

**Table 1.** Origin of equine SCC tumors

	<b>Signalment</b>	<b>Tumor Origin</b>	<b>Xenograft take rate</b>
<b>Tumor 1</b>	Appaloosa 12-year old mare	Cornea	1/15 (6.6%) SCID mouse
<b>Tumor 2</b>	Missouri Fox Trotting Horse 11-year-old gelding	Third eyelid	1/15 (6.6%) Nude mouse
<b>Tumor 3</b>	Thoroughbred 20-year-old mare	Bulbar conjunctiva	1/15 (6.6%) Nude mouse

**Table 2.** Experiment A – effect of photoactive drug dose

	<b>Verteporfin dose (mg/cm<sup>3</sup>)</b>	<b>Solvent</b>
<b>Treatment group A1</b>	0.01	DMSO
<b>Treatment group A2</b>	0.1	DMSO
<b>Treatment group A3</b>	1.0	DMSO
<b>Control group A4</b>	None	DMSO
<b>Control group A5</b>	None	None
<b>Control group A6</b>	0.1	DMSO

**Table 3.** Experiment B – effect of solvent

	<b>Verteporfin dose (mg/cm<sup>3</sup>)</b>	<b>Solvent</b>
<b>Treatment group B1</b>	0.1	D5W
<b>Treatment group B2</b>	0.1	DMSO
<b>Control group B3</b>	No drug	D5W
<b>Control group B4</b>	No drug	DMSO



## FIGURES

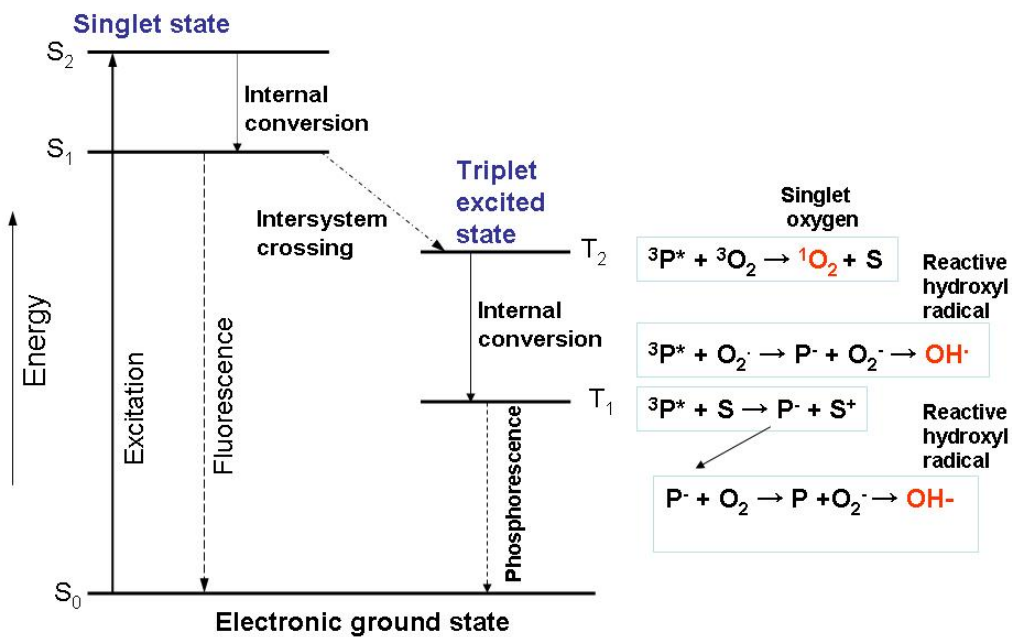


**Figure 1.** Jablonski diagram

<sup>3</sup>P\* triplet excited state photosensitizer, S oxidized substrate, <sup>3</sup>O<sub>2</sub> triplet ground state oxygen, O<sub>2</sub><sup>-</sup> superoxide anion, O<sub>2</sub><sup>·</sup> superoxide radical, P<sup>+</sup> oxydized photosensitizer, <sup>1</sup>O<sub>2</sub> singlet state oxygen.

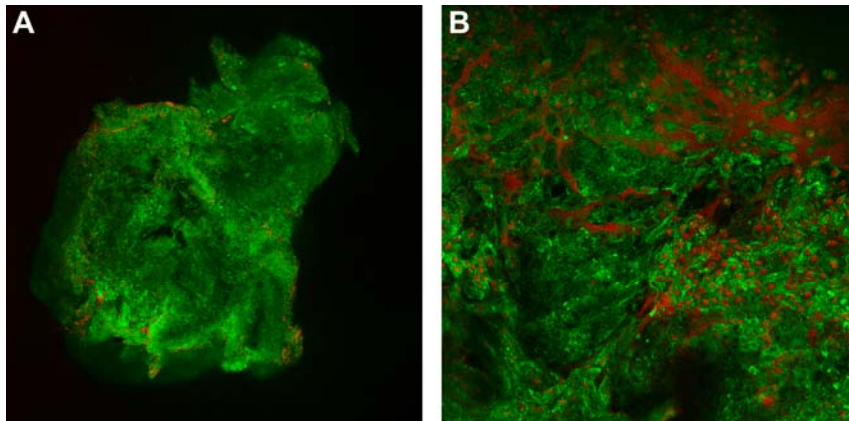


**Figure 2.** Confocal microscopy images of cryopreserved equine ocular SCC from one of the original equine patients, x 4 (A) , x 30 (B).



**Figure 3.** The SCID mouse bearing equine SCC 138 days following implantation.

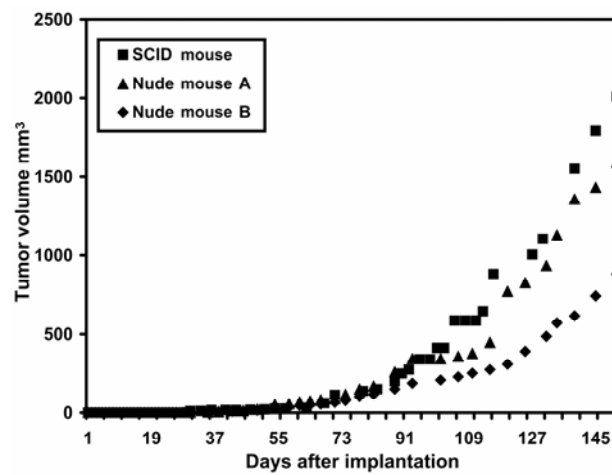


**Figure 4.** Growth curve of xenotransplanted equine SCC

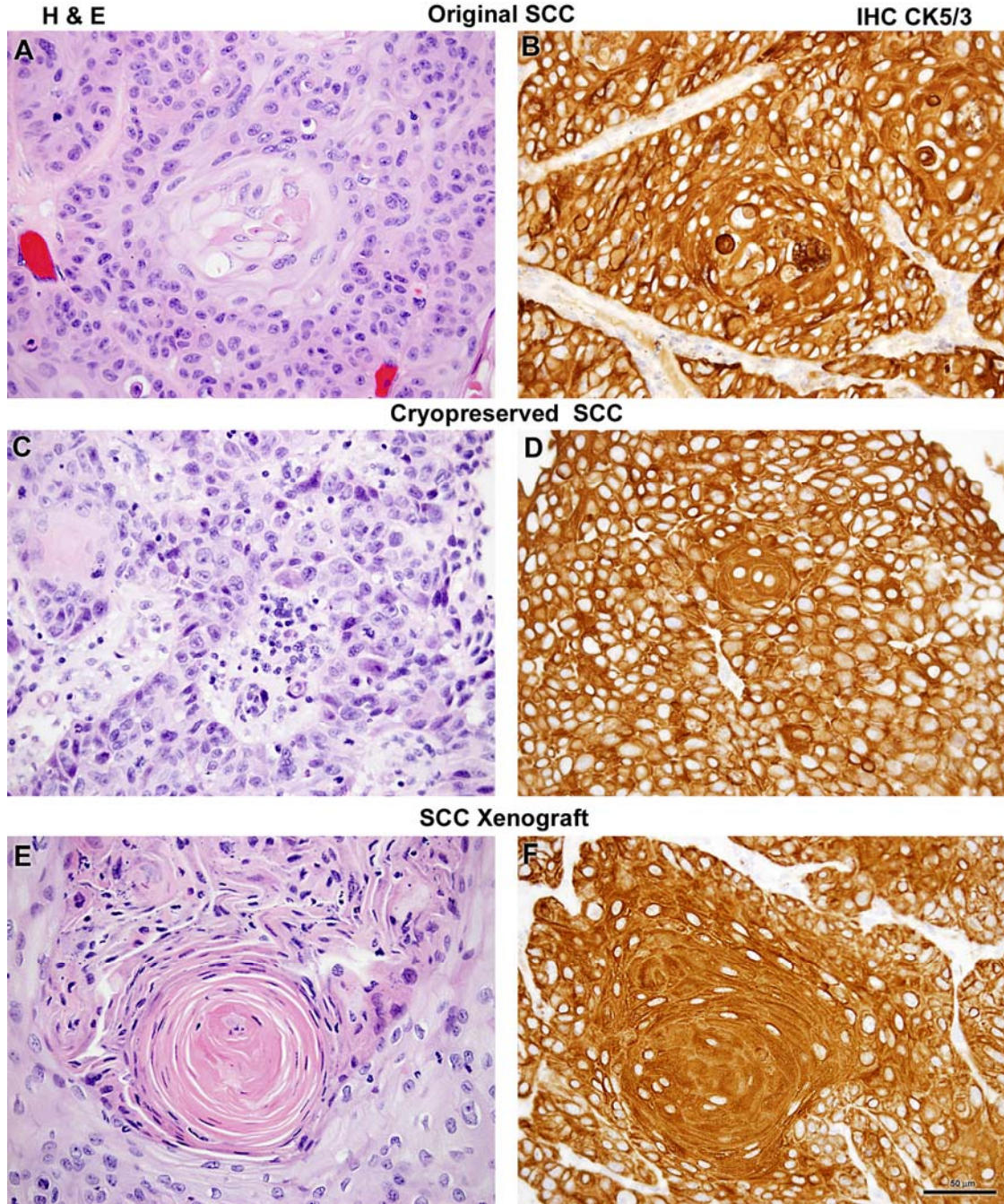


**Figure 5.** Histopathology of SCC from an original equine patient, H&E stain, x 400(A), immunohistochemical staining for cytokeratin 5/6 on SCC from an original equine patient, x 400 (B), histopathology of cryopreserved equine SCC, H&E stain, x 400(C), immunohistochemistry staining for cytokeratin 5/6 on a cryopreserved equine SCC, x 400 (D), histopathology of an equine xenograft harvested on day 150 from a SCID mouse, H&E stain, x 400 (E), immunohistochemical staining for cytokeratin 5/6 on a SCC xenograft, x 400 (F)

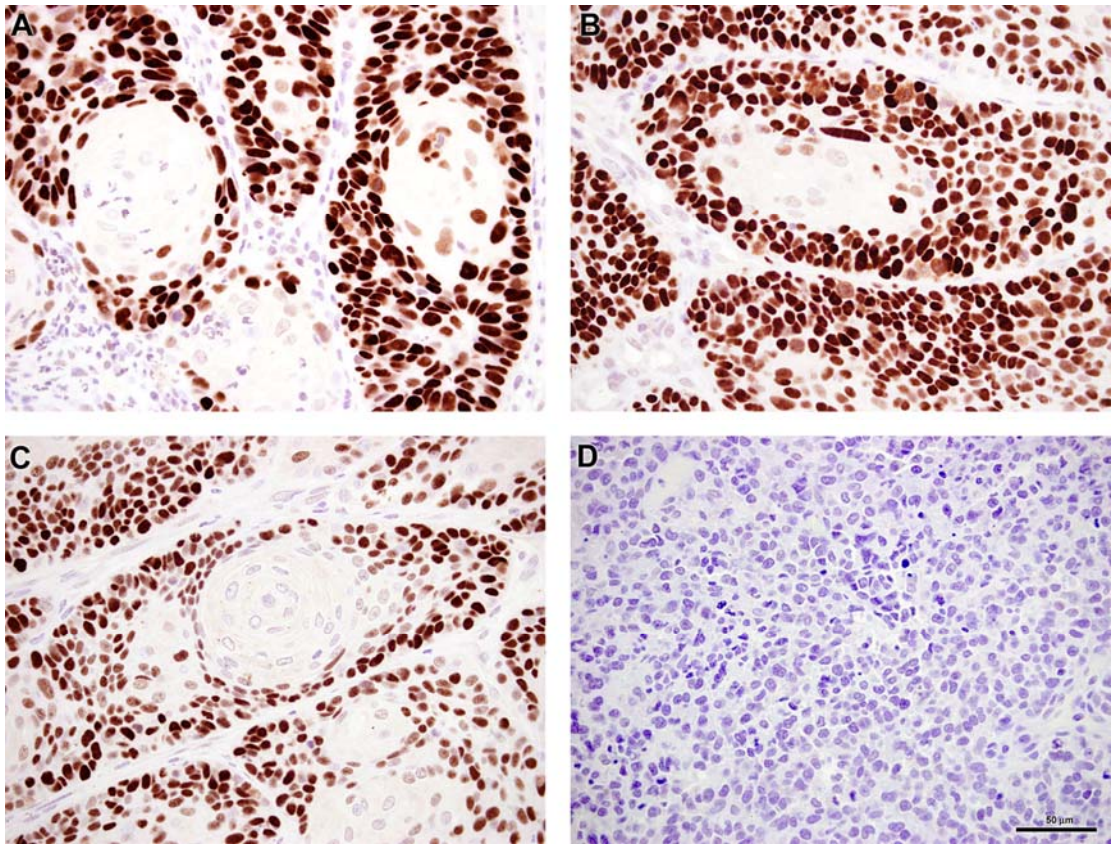


**Figure 6.** Immunoreactivity for p53 on original (A), cryopreserved (B), and transplanted (C) ocular SCC. Nonimmune control (D).

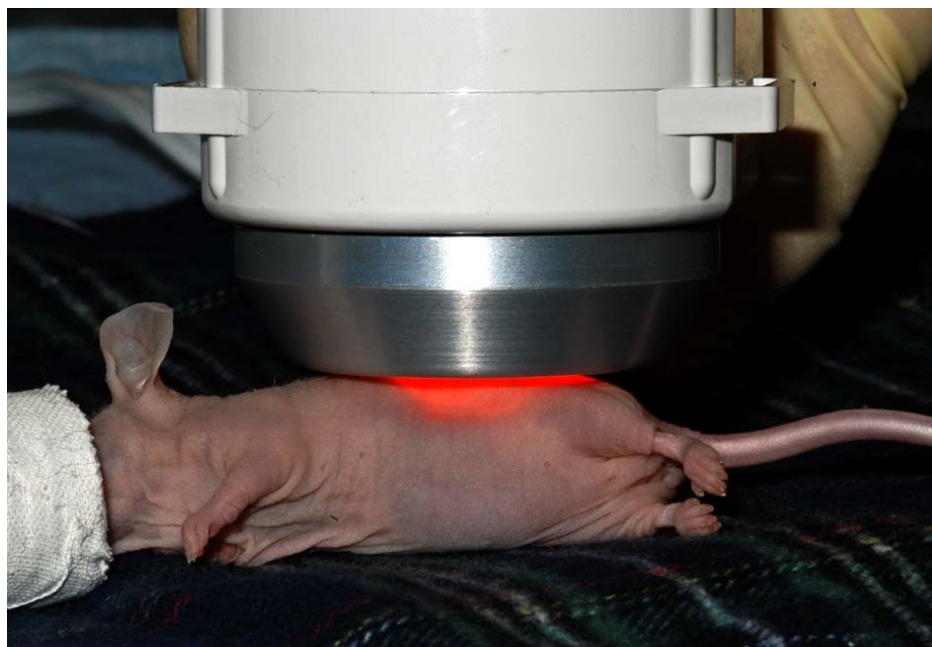
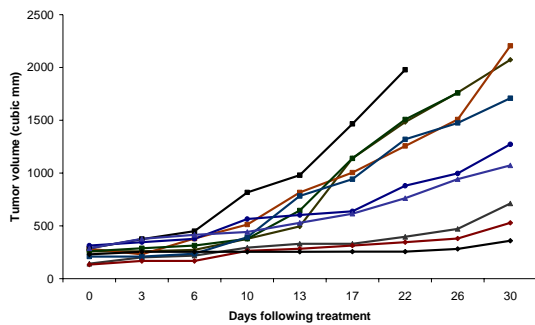


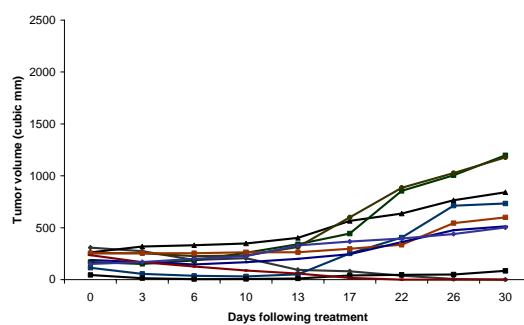
**Figure 7.** A photograph of a xenografted nude mouse under general anesthesia being illuminated with LED light after local injection with verteporfin.



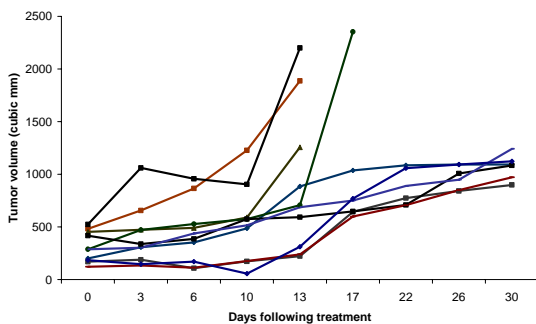
**Figure 8.** Photographs of an ulcer formed in the treatment site following PDT with local injection of verteporfin at a dose of  $0.1 \text{ mg/cm}^3$ .



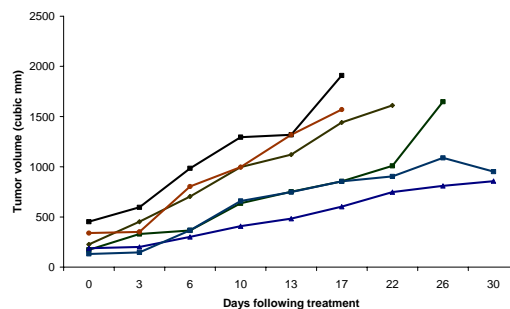
Treatment group A1



Treatment group A2

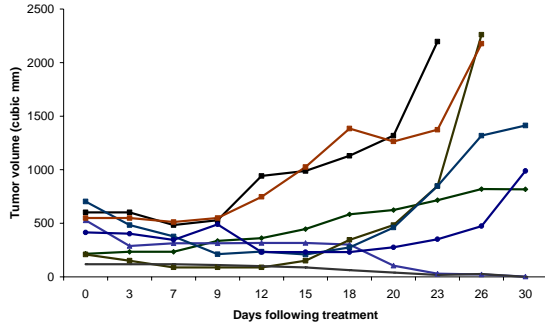


Control group A4

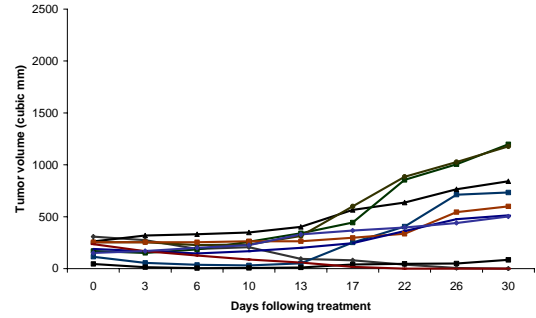


Control group A5

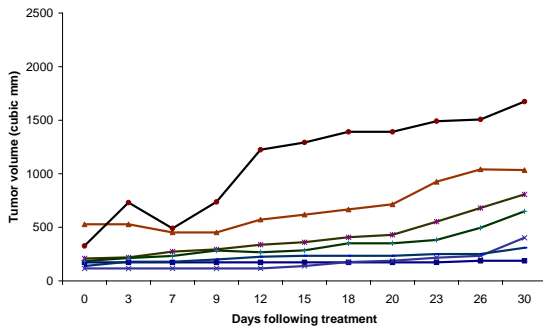
**Figure 9.** Comparison of tumor growth in experiment A.



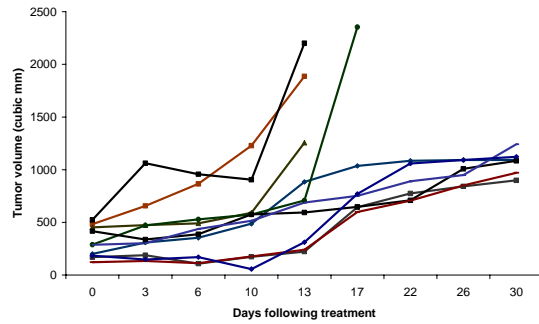
Treatment group B1



Treatment group B2



Control group B3



Control group B4

**Figure 10.** Comparison of tumor growth in experiment B.

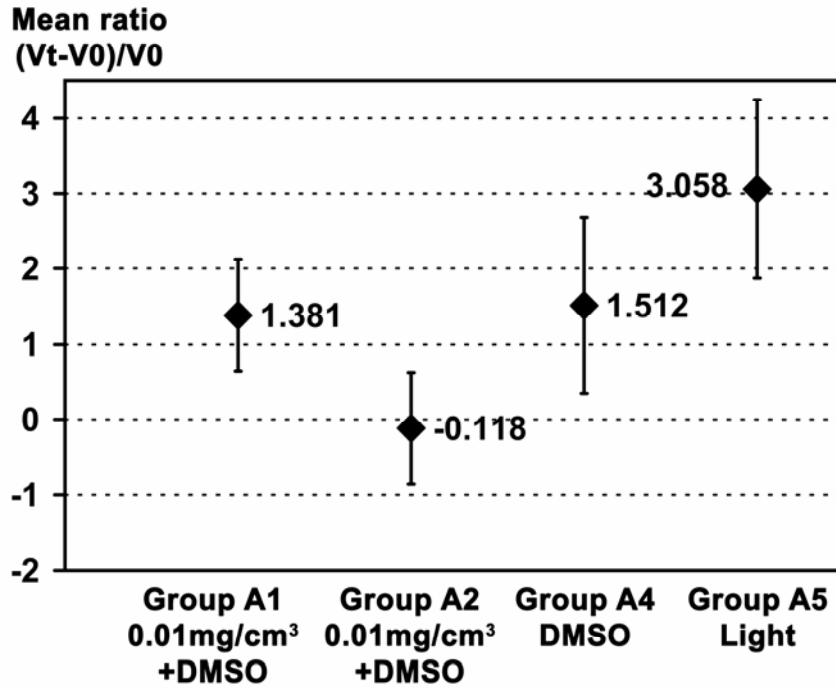


Figure 11. Experiment A. Mean relative change in tumor volume at day 13.

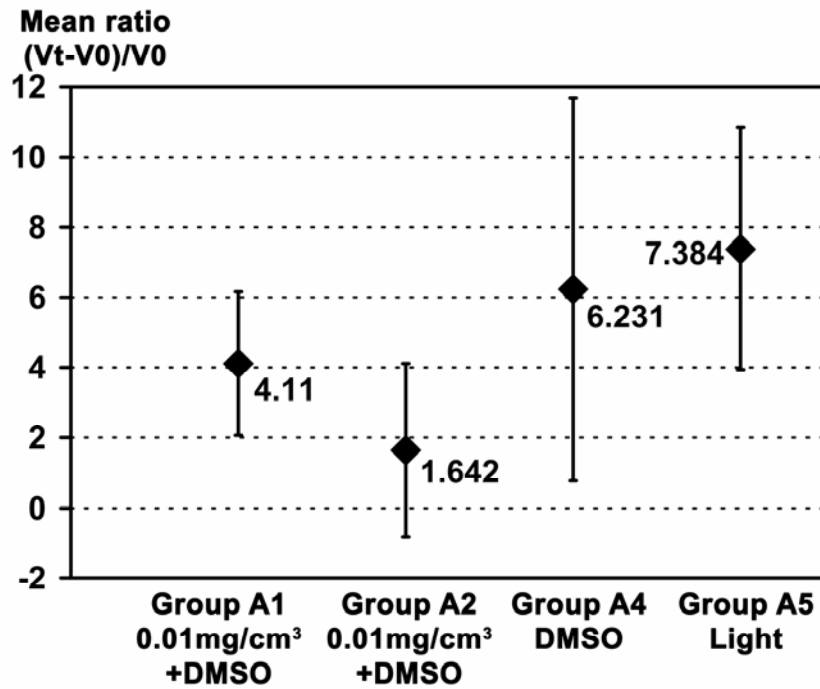


Figure 12. Experiment A. Mean relative change in tumor volume at day 30.



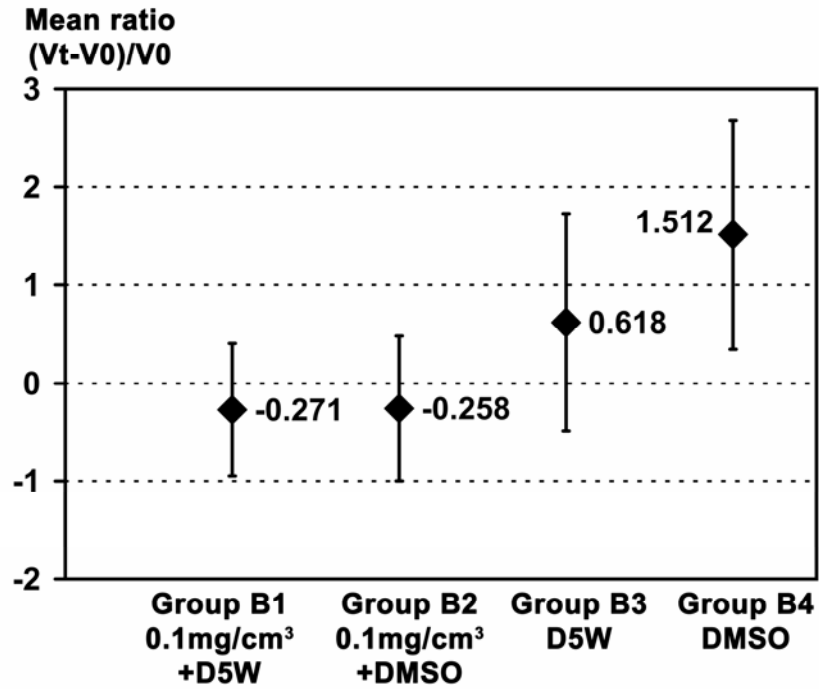


Figure 13. Experiment B. Mean relative change in tumor volume at day 13.

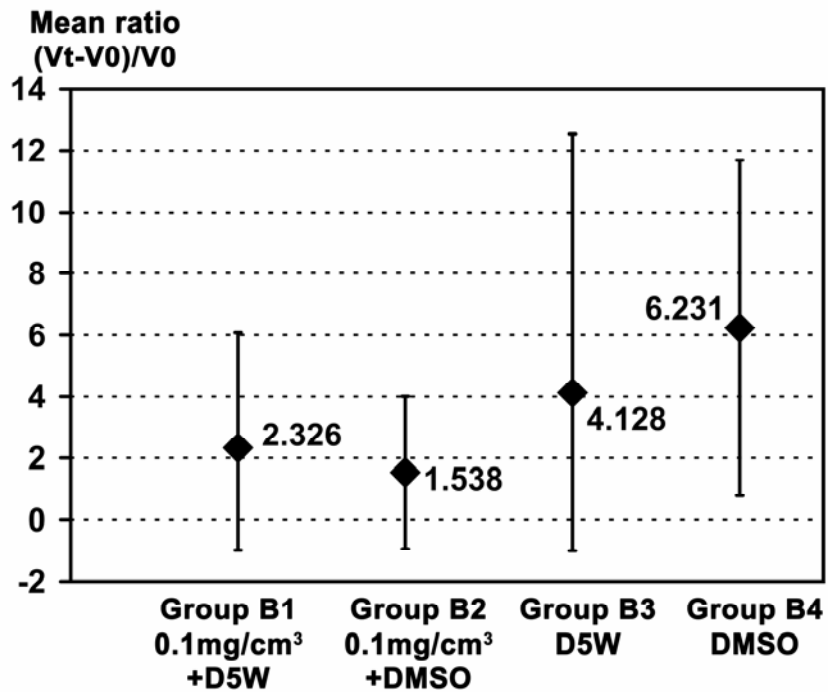


Figure 14. Experiment B. Mean relative change in tumor volume at day 30.



**Figure 15.** A Photograph of a mouse in treatment group B2 demonstrating complete regression of SCC. The mouse here, had an initial tumor of  $234.45 \text{ mm}^3$  at the time of treatment and was observed to be free of any gross evidence of SCC at day 20 (inset).

## BIBLIOGRAPHY

1. Lavach JD, Severin GA. Neoplasia of the equine eye, adnexa, and orbit: a review of 68 cases. *Journal of the American Veterinary Medical Association* 1977;170:202-203.
2. Junge RE, Sundberg JP, Lancaster WD. Papillomas and squamous cell carcinomas of horses. *Journal of the American Veterinary Medical Association* 1984;185:656-659.
3. King TC, Priehs DR, Gum GG, et al. Therapeutic management of ocular squamous cell carcinoma in the horse: 43 cases (1979-1989). *Equine Veterinary Journal* 1991;23:449-452.
4. Dugan SJ, Roberts SM, Curtis CR, et al. Prognostic factors and survival of horses with ocular/adnexal squamous cell carcinoma: 147 cases (1978-1988). *Journal of the American Veterinary Medical Association* 1991;198:298-303.
5. Gelatt KN, Myers VS, Jr., Perman V, et al. Conjunctival squamous cell carcinoma in the horse. *Journal of the American Veterinary Medical Association* 1974;165:617-620.
6. Schwink K. Factors influencing morbidity and outcome of equine ocular squamous cell carcinoma. *Equine Veterinary Journal* 1987;19:198-200.
7. Koch SA, Cowles RR, Jr. Surgical removal of squamous cell carcinoma of the equine eye. *Veterinary Medicine, Small Animal Clinician* 1971;66:327-329.
8. Hilbert BJ, Farrell RK, Grant BD. Cryotherapy of periocular squamous cell carcinoma in the horse. *Journal of the American Veterinary Medical Association* 1977;170:1305-1308.
9. Frauenfelder HC, Blevins WE, Page EH. <sup>90</sup>Sr for treatment of periocular squamous cell carcinoma in the horse. *Journal of the American Veterinary Medical Association* 1982;180:307-309.
10. Joyce JR. Cryosurgical treatment of tumors of horses and cattle. *Journal of the American Veterinary Medical Association* 1976;168:226-229.
11. Grier RL, Brewer WG, Jr., Paul SR, et al. Treatment of bovine and equine ocular squamous cell carcinoma by radiofrequency hyperthermia. *Journal of the American Veterinary Medical Association* 1980;177:55-61.
12. Theon AP, Pascoe JR, Carlson GP, et al. Intratumoral chemotherapy with cisplatin in oily emulsion in horses. *Journal American Veterinary Association* 1993;202:261-267.
13. Gavin PR, Gillette EL. Interstitial radiation therapy of equine squamous cell carcinoma. *Journal of American Veterinary Radiology* 1978;19:138-141.
14. Mosunic CB, Moore PA, Dietrich U, et al. A retrospective study of the treatment and prognosis of equine ocular squamous cell carcinoma. Proceedings of the 33rd Annual Meeting of the American College of Veterinary Ophthalmologists 2002;28.
15. Goldin A, Venditti JM, Macdonald JS, et al. Current results of the screening program at the Division of Cancer Treatment, National Cancer Institute. *Eur J Cancer* 1981;17:129-142.

16. Fiebig H, Burger, AM. *Human Tumor Xenografts and Explants*. Totowa, New Jersey: Humana Press, 2002.
17. Norval M, Maingay J, Else RW. Studies of three canine mammary cell lines--II. In vivo properties. *Eur J Cancer Clin Oncol* 1984;20:1501-1508.
18. Hammond WG, Benfield JR, Teplitz RL. Metastatic behaviour of canine lung carcinoma in autochthonous and xenotransplant hosts. *Clin Exp Metastasis* 1991;9:567-577.
19. Maruo K, Sugimoto T, Suzuki K, et al. Growth and metastasis of two canine mast cell tumors in SCID mice. *J Vet Med Sci* 1996;58:567-569.
20. Baron T, Dore JF. Transplantation of canine malignant lymphomas in the nude and SCID mouse. *In Vivo* 1992;6:77-79.
21. Baron T, Dore JF. Intra-cranial transplantation of canine malignant lymphomas in the nude mouse. *In Vivo* 1993;7:447-450.
22. Harmelin A, Pinthus JH, Katzir N, et al. Use of a murine xenograft model for canine transmissible venereal tumor. *Am J Vet Res* 2001;62:907-911.
23. Rainov NG, Koch S, Sena-Esteves M, et al. Characterization of a canine glioma cell line as related to established experimental brain tumor models. *J Neuropathol Exp Neurol* 2000;59:607-613.
24. Ladiges WC, Van Hoosier GL, Jr. Heterotransplantation of feline malignant tumors in nude thymusless mice. *Am J Vet Res* 1980;41:840-842.
25. Rasheed S. Characterization of a differentiated cat melanoma cell line. *Cancer Res* 1983;43:3379-3384.
26. Irvin AD, Brown CG, Kanhai GK, et al. Transplantation of bovine lymphosarcoma cells to athymic (nude) mice. *Res Vet Sci* 1977;22:53-55.
27. Al-Yaman F, Willenborg DO. Heterotransplantation of ovine squamous cell carcinomata into nude mice. *Res Vet Sci* 1984;36:339-344.
28. Pardini LL, Aaronson LM, Hering PL, et al. Heterotransplantation of equine carcinoma cells in athymic (nude) mice. *Am J Vet Res* 1986;47:610-614.
29. Fatemi-Nainie S, Anderson LW, Cheevers WP. Culture characteristics and tumorigenicity of the equine sarcoid-derived MC-1 cell line. *Am J Vet Res* 1984;45:1105-1108.
30. Muleya JS, Nakaichi M, Sugahara J, et al. Establishment and characterization of a new cell line derived from feline mammary tumor. *J Vet Med Sci* 1998;60:931-935.
31. Shimamoto Y, Kameya T, Nagai K, et al. Transplantation of human tumors in nude mice. *J Natl Cancer Inst* 1976;56:1251-1260.
32. Hill LL, Korngold R, Jaworsky C, et al. Growth and metastasis of fresh human melanoma tissue in mice with severe combined immunodeficiency. *Cancer Res* 1991;51:4937-4941.
33. Riddick AC, Barker C, Sheriffs I, et al. Banking of fresh-frozen prostate tissue: methods, validation and use. *BJU Int* 2003;91:315-323; discussion 323-314.
34. Huang Q, Sacks PG, Mo J, et al. A simple method for fixation and microdissection of frozen fresh tissue sections for molecular cytogenetic analysis of cancers. *Biotech Histochem* 2005;80:147-156.
35. Biel M. Advances in photodynamic therapy for the treatment of head and neck cancers. *Lasers Surg Med* 2006;38:349-355.

36. Sharp DM, Lai S, Markey CM. Photodynamic therapy with verteporfin for choroidal neovascularization due to age-related macular degeneration and other causes: a New Zealand outcomes study. *Clin Experiment Ophthalmol* 2007;35:24-31.
37. Tang G, Hyman S, Schneider JH, Jr., et al. Application of photodynamic therapy to the treatment of atherosclerotic plaques. *Neurosurgery* 1993;32:438-443; discussion 443.
38. Triesscheijn M, Baas P, Schellens JH, et al. Photodynamic therapy in oncology. *Oncologist* 2006;11:1034-1044.
39. MacDonald IJ, Dougherty TJ. Basic principles of photodynamic therapy. *Porphyrins and Phthalocyanines* 2001;5:105-129.
40. Dougherty TJ, Gomer CJ, Henderson BW, et al. Photodynamic Therapy. *Journal of the National Cancer Institute* 1998;90:889-905.
41. Evans HH, Horng MF, Ricanati M, et al. Mutagenicity of photodynamic therapy as compared to UVC and ionizing radiation in human and murine lymphoblast cell lines. *Photochem Photobiol* 1997;66:690-696.
42. Marcus SL, McIntyre WR. Photodynamic therapy systems and applications. *Expert Opin Emerg Drugs* 2002;7:321-334.
43. CS F. *Mechanisms of photo-oxygenation*. New York: Alan R. Liss, 1984.
44. Kessel D, Woodburn K. Biodistribution of photosensitizing agents. *Int J Biochem* 1993;25:1377-1383.
45. Gaullier JM, Geze M, Santus R, et al. Subcellular localization of and photosensitization by protoporphyrin IX human keratinocytes and fibroblasts cultivated with 5-aminolevulinic acid. *Photochem Photobiol* 1995;62:114-122.
46. Woodburn KW, Vardaxis NJ, Hill JS, et al. Subcellular localization of porphyrins using confocal laser scanning microscopy. *Photochem Photobiol* 1991;54:725-732.
47. Geze M, Morliere P, Maziere JC, et al. Lysosomes, a key target of hydrophobic photosensitizers proposed for photochemotherapeutic applications. *J Photochem Photobiol B* 1993;20:23-35.
48. Moan J, Berg K, Anholt H, et al. Sulfonated aluminium phthalocyanines as sensitizers for photochemotherapy. Effects of small light doses on localization, dye fluorescence and photosensitivity in V79 cells. *Int J Cancer* 1994;58:865-870.
49. Hilf R, Warne NW, Smail DB, et al. Photodynamic inactivation of selected intracellular enzymes by hematoporphyrin derivative and their relationship to tumor cell viability in vitro. *Cancer Lett* 1984;24:165-172.
50. Miccoli L, Beurdeley-Thomas A, De Pinieux G, et al. Light-induced photoactivation of hypericin affects the energy metabolism of human glioma cells by inhibiting hexokinase bound to mitochondria. *Cancer Res* 1998;58:5777-5786.
51. Agarwal ML, Clay ME, Harvey EJ, et al. Photodynamic therapy induces rapid cell death by apoptosis in L5178Y mouse lymphoma cells. *Cancer Res* 1991;51:5993-5996.
52. He J, Agarwal ML, Larkin HE, et al. The induction of partial resistance to photodynamic therapy by the protooncogene BCL-2. *Photochem Photobiol* 1996;64:845-852.
53. Kim HR, Luo Y, Li G, et al. Enhanced apoptotic response to photodynamic therapy after bcl-2 transfection. *Cancer Res* 1999;59:3429-3432.

54. Perlin DS, Murant RS, Gibson SL, et al. Effects of photosensitization by hematoporphyrin derivative on mitochondrial adenosine triphosphatase-mediated proton transport and membrane integrity of R3230AC mammary adenocarcinoma. *Cancer Res* 1985;45:653-658.
55. Henderson BW, Dougherty TJ. How does photodynamic therapy work? *Photochemistry & Photobiology* 1992;55:145-157.
56. Schmidt-Erfurth U, Hasan T. Mechanisms of action of photodynamic therapy with verteporfin for the treatment of age-related macular degeneration. *Surv Ophthalmol* 2000;45:195-214.
57. Henderson BW, Fingar VH. Relationship of tumor hypoxia and response to photodynamic treatment in an experimental mouse tumor. *Cancer Res* 1987;47:3110-3114.
58. Henderson BW, Waldow SM, Mang TS, et al. Tumor destruction and kinetics of tumor cell death in two experimental mouse tumors following photodynamic therapy. *Cancer Res* 1985;45:572-576.
59. Chaudhuri K, Keck RW, Selman SH. Morphological changes of tumor microvasculature following hematoporphyrin derivative sensitized photodynamic therapy. *Photochem Photobiol* 1987;46:823-827.
60. Gilissen MJ, van de Merbel-de Wit LE, Star WM, et al. Effect of photodynamic therapy on the endothelium-dependent relaxation of isolated rat aortas. *Cancer Res* 1993;53:2548-2552.
61. Henderson BW, Fingar VH. Oxygen limitation of direct tumor cell kill during photodynamic treatment of a murine tumor model. *Photochem Photobiol* 1989;49:299-304.
62. Star WM, Marijnissen HP, van den Berg-Blok AE, et al. Destruction of rat mammary tumor and normal tissue microcirculation by hematoporphyrin derivative photoradiation observed in vivo in sandwich observation chambers. *Cancer Res* 1986;46:2532-2540.
63. Nelson JS, Liaw LH, Orenstein A, et al. Mechanism of tumor destruction following photodynamic therapy with hematoporphyrin derivative, chlorin, and phthalocyanine. *J Natl Cancer Inst* 1988;80:1599-1605.
64. Chen Q, Chen H, Hetzel FW. Tumor oxygenation changes post-photodynamic therapy. *Photochem Photobiol* 1996;63:128-131.
65. Korbelik M. Induction of tumor immunity by photodynamic therapy. *J Clin Laser Med Surg* 1996;14:329-334.
66. Fingar VH. Vascular effects of photodynamic therapy. *J Clin Laser Med Surg* 1996;14:323-328.
67. Ochsner M. Photophysical and photobiological processes in the photodynamic therapy of tumours. *J Photochem Photobiol B* 1997;39:1-18.
68. Gollnick SO, Liu X, Owczarczak B, et al. Altered expression of interleukin 6 and interleukin 10 as a result of photodynamic therapy in vivo. *Cancer Res* 1997;57:3904-3909.
69. Kros G, Korbelik M, Dougherty GJ. Induction of immune cell infiltration into murine SCCVII tumour by photofrin-based photodynamic therapy. *Br J Cancer* 1995;71:549-555.

70. Korbelik M, Dougherty GJ. Photodynamic therapy-mediated immune response against subcutaneous mouse tumors. *Cancer Res* 1999;59:1941-1946.
71. Korbelik M, Krosil G, Krosil J, et al. The role of host lymphoid populations in the response of mouse EMT6 tumor to photodynamic therapy. *Cancer Res* 1996;56:5647-5652.
72. Luksiene Z. Photodynamic therapy: mechanism of action and ways to improve the efficiency of treatment. *Medicina (Kaunas)* 2003;39:1137-1150.
73. Korbelik M, Krosil G, Chaplin DJ. Photofrin uptake by murine macrophages. *Cancer Res* 1991;51:2251-2255.
74. Korbelik M, Krosil G, Olive PL, et al. Distribution of Photofrin between tumour cells and tumour associated macrophages. *Br J Cancer* 1991;64:508-512.
75. Barrett AJ, Kennedy JC, Jones RA, et al. The effect of tissue and cellular pH on the selective biodistribution of porphyrin-type photochemotherapeutic agents: a volumetric titration study. *J Photochem Photobiol B* 1990;6:309-323.
76. Freitas I. Lipid accumulation: the common feature to photosensitizer-retaining normal and malignant tissues. *J Photochem Photobiol B* 1990;7:359-361.
77. Musser DA, Wagner JM, Datta-Gupta M. The interaction of tumor localizing porphyrins with collagen and elastin. *Research Communications in Chemical Pathology & Pharmacology* 1982;36:251-259.
78. Hamblin MR, Newman EL. Photosensitizer targeting in photodynamic therapy. II. Conjugates of haematoporphyrin with serum lipoproteins. *J Photochem Photobiol B* 1994;26:147-157.
79. Mosley ST, Goldstein JL, Brown MS, et al. Targeted killing of cultured cells by receptor-dependent photosensitization. *Proc Natl Acad Sci U S A* 1981;78:5717-5721.
80. Jori G. Tumour photosensitizers: approaches to enhance the selectivity and efficiency of photodynamic therapy. *J Photochem Photobiol B* 1996;36:87-93.
81. Allison BA, Pritchard PH, Levy JG. Evidence for low-density lipoprotein receptor-mediated uptake of benzoporphyrin derivative. *Br J Cancer* 1994;69:833-839.
82. Grossweiner LI. Photodynamic therapy. *J Laser Appl* 1995;7:51-57.
83. Moan J, Sommer S. Uptake of the components of hematoporphyrin derivative by cells and tumours. *Cancer Lett* 1983;21:167-174.
84. Hamblin MR, Newman EL. On the mechanism of the tumour-localising effect in photodynamic therapy. *J Photochem Photobiol B* 1994;23:3-8.
85. Chen M, Pennathur A, Luketich JD. Role of photodynamic therapy in unresectable esophageal and lung cancer. *Lasers Surg Med* 2006;38:396-402.
86. Pandey RK, Bellnier DA, Smith KM, et al. Chlorin and Porphyrin Derivatives as Potential Photosensitizers in Photodynamic Therapy. *Photochemistry & Photobiology* 1991;53:65-72.
87. Sternberg ED, Dolphin D. Second generation photodynamic agents: a review. *J Clin Laser Med Surg* 1993;11:233-241.
88. Aveline B, Hasan T, Redmond RW. Photophysical and photosensitizing properties of benzoporphyrin derivative monoacid ring A (BPD-MA). *Photochem Photobiol* 1994;59:328-335.

89. Petermeier K, Tatar O, Inhoffen W, et al. Verteporfin photodynamic therapy induced apoptosis in choroidal neovascular membranes. *Br J Ophthalmol* 2006;90:1034-1039.
90. Houle JM, Strong A. Clinical pharmacokinetics of verteporfin. *J Clin Pharmacol* 2002;42:547-557.
91. Richter AM, Cerruti-Sola S, Sternberg ED, et al. Biodistribution of tritiated benzoporphyrin derivative (3H-BPD-MA), a new potent photosensitizer, in normal and tumor-bearing mice. *J Photochem Photobiol B* 1990;5:231-244.
92. Lui H, Hobbs L, Tope WD, et al. Photodynamic therapy of multiple nonmelanoma skin cancers with verteporfin and red light-emitting diodes: two-year results evaluating tumor response and cosmetic outcomes. *Arch Dermatol* 2004;140:26-32.
93. Brancalion L, Moseley H. Laser and non-laser light sources for photodynamic therapy. *Lasers Med Sci* 2002;17:173-186.
94. Keijzer M, Jacques SL, Prahl SA, et al. Light distributions in artery tissue: Monte Carlo simulations for finite-diameter laser beams. *Lasers Surg Med* 1989;9:148-154.
95. Pogue BW, Momma T, Wu HC, et al. Transient absorption changes in vivo during photodynamic therapy with pulsed-laser light. *Br J Cancer* 1999;80:344-351.
96. Bernstein EF, Thomas GF, Smith PD, et al. Response of black and white guinea pig skin to photodynamic treatment using 514-nm light and dihematoporphyrin ether. *Arch Dermatol* 1990;126:1303-1307.
97. Giuliano EA MI, Johnson PJ. Photodynamic therapy for the treatment of periocular squamous cell carcinoma in horses. 34th Annu Meet ACVO 2003;69.
98. Klauss G GE, McCaw DL, MacDonald I, Johnson PJ, Galle LE, Moore CP. Treatment of equine periocular squamous cell carcinoma with photodynamic therapy; 5 cases. 35 th Annu Meet ACVO 2004;10.
99. Bavister BD, Leibfried ML, Lieberman G. Development of preimplantation embryos of the golden hamster in a defined culture medium. *Biology of Reproduction* 1983;28:235-247.
100. Bosma GC, Davisson MT, Ruetsch NR, et al. The mouse mutation severe combined immune deficiency (scid) is on chromosome 16. *Immunogenetics* 1989;29:54-57.
101. Meck RA, Ingram M, Meck JM, et al. Establishment and cell cycle kinetics of a human squamous cell carcinoma in nude mice and in vitro. *Cancer Res* 1981;41:1076-1085.
102. Sharkey FE, Fogh J. Considerations in the use of nude mice for cancer research. *Cancer Metastasis Rev* 1984;3:341-360.
103. Sugimoto T, Maruo K, Imaeda Y, et al. Xenotransplantation of canine tumors into severe combined immunodeficient (SCID) mice. *J Vet Med Sci* 1994;56:1087-1091.
104. Braakhuis BJ, Sneeuwloper G, Snow GB. The potential of the nude mouse xenograft model for the study of head and neck cancer. *Arch Otorhinolaryngol* 1984;239:69-79.



105. Inohara H, Matsunaga T, Nomura T. Growth and metastasis of fresh human benign and malignant tumors in the head and neck regions transplanted into scid mice. *Carcinogenesis* 1992;13:845-849.
106. Corbett TH PL, Roberts BJ. *Transplantable Syngeneic Rodent Tumors*. Totowa, New Jersey: Human Press, 2002.
107. Jensen HM, Wellings SR. Preneoplastic lesions of the human mammary gland transplanted into the nude athymic mouse. *Cancer Res* 1976;36:2605-2610.
108. Gershwin ME, Ikeda RM, Kawakami TG, et al. Immunobiology of heterotransplanted human tumors in nude mice. *J Natl Cancer Inst* 1977;58:1455-1461.
109. Kopf-Maier P. Dying and regeneration of human tumor cells after heterotransplantation to athymic mice. *Histol Histopathol* 1986;1:383-390.
110. Picard O, Rolland Y, Poupon MF. Fibroblast-dependent tumorigenicity of cells in nude mice: implication for implantation of metastases. *Cancer Res* 1986;46:3290-3294.
111. Gartner MF, Wilson EL, Dowdle EB. Fibroblast-dependent tumorigenicity of melanoma xenografts in athymic mice. *Int J Cancer* 1992;51:788-791.
112. Wallace AC. Effect Of Delayed Addition Of Irradiated Cells To Small Viable Tumor Inocula. *Cancer Res* 1965;25:355-357.
113. Xie X, Brunner N, Jensen G, et al. Comparative studies between nude and scid mice on the growth and metastatic behavior of xenografted human tumors. *Clin Exp Metastasis* 1992;10:201-210.
114. Azar HA, Hansen CT, Costa J. N:NIH(S)-nu/nu mice with combined immunodeficiency: a new model for human tumor heterotransplantation. *J Natl Cancer Inst* 1980;65:421-430.
115. Fogh J, Tiso J, Orfeo T, et al. Thirty-four lines of six human tumor categories established in nude mice. *J Natl Cancer Inst* 1980;64:745-751.
116. Taylor CW, Grogan TM, Lopez MH, et al. Growth and dissemination of human malignant melanoma cells in mice with severe combined immune deficiency. *Lab Invest* 1992;67:130-137.
117. Al-Yaman F, Willenborg DO. Successful isolation, cultivation and partial characterization of naturally occurring ovine squamous cell carcinoma. *Vet Immunol Immunopathol* 1984;5:273-288.
118. Shimada Y, Maeda M, Watanabe G, et al. Cell culture in esophageal squamous cell carcinoma and the association with molecular markers. *Clin Cancer Res* 2003;9:243-249.
119. Dahm AM, de Bruin A, Linat A, et al. Cultivation and characterisation of primary and subcultured equine keratinocytes. *Equine Vet J* 2002;34:114-120.
120. Rheinwald JG, Beckett MA. Tumorigenic keratinocyte lines requiring anchorage and fibroblast support cultures from human squamous cell carcinomas. *Cancer Res* 1981;41:1657-1663.
121. Ballo H, Koldovsky P, Hoffmann T, et al. Establishment and characterization of four cell lines derived from human head and neck squamous cell carcinomas for an autologous tumor-fibroblast in vitro model. *Anticancer Res* 1999;19:3827-3836.

122. Suter MM, Pantano DM, Flanders JA, et al. Comparison of growth and differentiation of normal and neoplastic canine keratinocyte cultures. *Vet Pathol* 1991;28:131-138.
123. Sarbia M, Bosing N, Hildebrandt B, et al. Characterization of two newly established cell lines derived from squamous cell carcinomas of the oesophagus. *Anticancer Res* 1997;17:2185-2192.
124. Tanaka H, Shibagaki I, Shimada Y, et al. Characterization of p53 gene mutations in esophageal squamous cell carcinoma cell lines: increased frequency and different spectrum of mutations from primary tumors. *Int J Cancer* 1996;65:372-376.
125. Hibino Y, Hata K, Horie K, et al. Structural changes and cell viability of cultured epithelium after freezing storage. *J Craniomaxillofac Surg* 1996;24:346-351.
126. Baust JM, Van Buskirk R, Baust JG. Modulation of the cryopreservation cap: elevated survival with reduced dimethyl sulfoxide concentration. *Cryobiology* 2002;45:97-108.
127. Baust JM, Vogel MJ, Van Buskirk R, et al. A molecular basis of cryopreservation failure and its modulation to improve cell survival. *Cell Transplant* 2001;10:561-571.
128. Ahn HJ, Sohn IP, Kwon HC, et al. Characteristics of the cell membrane fluidity, actin fibers, and mitochondrial dysfunctions of frozen-thawed two-cell mouse embryos. *Mol Reprod Dev* 2002;61:466-476.
129. Martin G, Sabido O, Durand P, et al. Cryopreservation induces an apoptosis-like mechanism in bull sperm. *Biol Reprod* 2004;71:28-37.
130. Teifke JP, Lohr CV. Immunohistochemical detection of P53 overexpression in paraffin wax-embedded squamous cell carcinomas of cattle, horses, cats and dogs. *J Comp Pathol* 1996;114:205-210.
131. Sironi G, Riccaboni P, Mertel L, et al. p53 protein expression in conjunctival squamous cell carcinomas of domestic animals. *Vet Ophthalmol* 1999;2:227-231.
132. Carvalho T, Vala H, Pinto C, et al. Immunohistochemical studies of epithelial cell proliferation and p53 mutation in bovine ocular squamous cell carcinoma. *Vet Pathol* 2005;42:66-73.
133. Shorthouse AJ, Smyth JF, Steel GG, et al. The human tumour xenograft--a valid model in experimental chemotherapy? *Br J Surg* 1980;67:715-722.
134. Sorensen AG, Patel S, Harmath C, et al. Comparison of diameter and perimeter methods for tumor volume calculation. *J Clin Oncol* 2001;19:551-557.
135. Tsoukas MM, Gonzalez S, Flotte TJ, et al. Wavelength and fluence effect on vascular damage with photodynamic therapy on skin. *J Invest Dermatol* 2000;114:303-308.
136. Panjehpour M, DeNovo RC, Petersen MG, et al. Photodynamic therapy using Verteporfin (benzoporphyrin derivative monoacid ring A, BPD-MA) and 630 nm laser light in canine esophagus. *Lasers Surg Med* 2002;30:26-30.
137. Marcus J, Glassberg E, Dimino-Emme L, et al. Photodynamic therapy for the treatment of squamous cell carcinoma using benzoporphyrin derivative. *J Dermatol Surg Oncol* 1994;20:375-382.

138. Gibson SL, van der Meid KR, Murant RS, et al. Increased efficacy of photodynamic therapy of R3230AC mammary adenocarcinoma by intratumoral injection of Photofrin II. *Br J Cancer* 1990;61:553-557.
139. Kostron H, Bellnier DA, Lin CW, et al. Distribution, retention, and phototoxicity of hematoporphyrin derivative in a rat glioma. Intraneoplastic versus intraperitoneal injection. *J Neurosurg* 1986;64:768-774.
140. Ceburkov O, Gollnick H. Photodynamic therapy in dermatology. *Eur J Dermatol* 2000;10:568-575; discussion 576.
141. Pogue BW, O'Hara JA, Demidenko E, et al. Photodynamic therapy with verteporfin in the radiation-induced fibrosarcoma-1 tumor causes enhanced radiation sensitivity. *Cancer Res* 2003;63:1025-1033.
142. Jiang F, Robin AM, Katakowski M, et al. Photodynamic therapy with photofrin in combination with Buthionine Sulfoximine (BSO) of human glioma in the nude rat. *Lasers Med Sci* 2003;18:128-133.
143. Inoue T, Ishida T, Sugio K, et al. Glutathione S transferase Pi is a powerful indicator in chemotherapy of human lung squamous-cell carcinoma. *Respiration* 1995;62:223-227.
144. Ferrario A, Gomer CJ. Systemic toxicity in mice induced by localized porphyrin photodynamic therapy. *Cancer Res* 1990;50:539-543.
145. Magne ML, Rodriguez CO, Autry SA, et al. Photodynamic therapy of facial squamous cell carcinoma in cats using a new photosensitizer. *Lasers in Surgery & Medicine* 1997;20:202-209.
146. Lin CW, Amano T, Rutledge AR, et al. Photodynamic effect in an experimental bladder tumor treated with intratumor injection of hematoporphyrin derivative. *Cancer Res* 1988;48:6115-6120.
147. Amano T, Prout GR, Jr., Lin CW. Intratumor injection as a more effective means of porphyrin administration for photodynamic therapy. *J Urol* 1988;139:392-395.
148. Misch DW, Misch MS. The effect of dimethyl sulfoxide on a lysosomal membrane. *Ann N Y Acad Sci* 1975;243:54-59.
149. Jacob SW, Herschler R. Dimethyl sulfoxide after twenty years. *Ann N Y Acad Sci* 1983;411:xiii-xvii.
150. Brayton CF. Dimethyl sulfoxide (DMSO): a review. *Cornell Vet* 1986;76:61-90.
151. Kharasch N, Thyagarajan BS. Structural basis for biological activities of dimethyl sulfoxide. *Ann N Y Acad Sci* 1983;411:391-402.
152. David NA. The pharmacology of dimethyl sulfoxide. *Annu Rev Pharmacol* 1972;12:353-374.
153. Wilson BC, Jeeves WP, Lowe DM. In vivo and post mortem measurements of the attenuation spectra of light in mammalian tissues. *Photochem Photobiol* 1985;42:153-162.
154. Okunaka T, Kato H, Konaka C, et al. A comparison between argon-dye and excimer-dye laser for photodynamic effect in transplanted mouse tumor. *Jpn J Cancer Res* 1992;83:226-231.
155. Beck ER CJ, Toung C. Clinically relevant dosimetry system for photodynamic therapy. *Veterinary Cancer Society* 1993;118-119.

156. Tralau CJ, MacRobert AJ, Coleridge-Smith PD, et al. Photodynamic therapy with phthalocyanine sensitisation: quantitative studies in a transplantable rat fibrosarcoma. *Br J Cancer* 1987;55:389-395.
157. Hahn KA, Panjehpour M, Legendre AM. Photodynamic therapy response in cats with cutaneous squamous cell carcinoma as a function of fluence. *Veterinary Dermatology* 1998;9:3-7.
158. Sitnik TM, Hampton JA, Henderson BW. Reduction of tumour oxygenation during and after photodynamic therapy in vivo: effects of fluence rate. *Br J Cancer* 1998;77:1386-1394.
159. Liu L, Trimarchi JR, Keefe DL. Involvement of mitochondria in oxidative stress-induced cell death in mouse zygotes. *Biol Reprod* 2000;62:1745-1753.
160. Stell AJ, Dobson JM, Langmack K. Photodynamic therapy of feline superficial squamous cell carcinoma using topical 5-aminolaevulinic acid. *Journal of Small Animal Practice* 2001;42:164-169.
161. Ota J GE, Mullen SF, Lewis MR, Cohn LA, Turk JR, Critser J, Moore CP. Xenotransplantation of cryopreserved equine squamous cell carcinoma to athymic nude and SCID mice. *Research in Veterinary Science* 2006;doi:10.1016/j.rvsc.2006.